

---

# THE PARTIAL $K$ FUNCTION

---

A PREPRINT

✉ **J. P. GRAINGER**<sup>\*1</sup>, ✉ **T. A. RAJALA**<sup>†2</sup>, ✉ **D. J. MURRELL**<sup>‡3</sup>, and ✉ **S. C. OLHEDE**<sup>§1</sup>

<sup>1</sup>Institute of Mathematics, École Polytechnique Fédérale de Lausanne, Station 8, 1015 Lausanne, Switzerland

<sup>2</sup>Natural Resources Institute Finland, 00790 Helsinki, Finland

<sup>3</sup>Research Department of Genetics, Evolution and Environment, Centre for Biodiversity and Environment Research, University College London, UK

December 2, 2025

## ABSTRACT

The  $K$  function and its related statistics have been an enduring tool in the analysis of spatial point processes, providing an easy to compute and interpret summary statistic for characterising the interactions between points of one type, or between two different types of points. In this paper, introduce a partial  $K$  function, enabling us to account for some of the effects of the other point types when analysing point-point interactions. The partial  $K$  function we introduce reduces to the usual  $K$  function when the other points are independent of the points of interest and has a similar interpretation. Using examples, we demonstrate how the partial  $K$  function can unpick dependence between point types that would otherwise be hidden in the usual  $K$  function. We also discuss important bias correction steps and hyperparameter selection. In addition, we discuss an extension to account for other spatial covariates, and demonstrate the methodology on the Lansing Woods dataset.

## 1 Introduction

Point patterns often arise from systems with complicated interactions between different types of points, for example, we might record the locations of individuals of multiple species of tree in a forest, all of which influence each other. Functional summary statistics, such as the  $K$  function (Ripley, 1977), provide a useful way to explore such interactions. Existing approaches perform well when we are interested in one or two types of points, and have been modified to account for covariates and long scale inhomogeneity (Baddeley et al., 2000). However, if there are more than two types of points present we may want to also account for the influence of these additional types of points. In particular, the influence of a third type of point may cause spurious clustering or repulsion between the two types of interest. For example, say we have three types of points,  $X$ ,  $Y$  and  $Z$ . If points of type  $X$  and type  $Y$  both cluster around points of type  $Z$ , then we may observe clustering between  $X$  and  $Y$  even if there is no direct interaction between them. This limitation of the existing  $K$  function is what we aim to address in this paper.

In this paper, we introduce partial versions of the standard second-order statistics used in the point process literature, in particular, any which can be computed from Ripley's  $K$  function. This complements the basic  $K$  function and the intensity-reweighted  $K$  function (Baddeley et al., 2000) with the new *partial  $K$  function*. The partial  $K$  function is particularly useful if we suspect that interactions between or within types could be due to the influence of other types of points, but we do not have a good model *a priori* to describe such dependence. If we have two types of points of interest,  $X$  and  $Y$ , Ripley's  $K$  function is informally

$$K_{XY}(r) = \frac{1}{\lambda_X} \mathbb{E} \left[ \begin{array}{l} \text{number of extra points of type } X \text{ within} \\ \text{a distance } r \text{ of a typical point of type } Y \end{array} \right],$$

---

<sup>\*</sup>[jake.grainger@epfl.ch](mailto:jake.grainger@epfl.ch)

<sup>†</sup>[tuomas.rajala@luke.fi](mailto:tuomas.rajala@luke.fi)

<sup>‡</sup>[d.murrell@ucl.ac.uk](mailto:d.murrell@ucl.ac.uk)

<sup>§</sup>[sofia.ohlhede@epfl.ch](mailto:sofia.ohlhede@epfl.ch)

where  $\lambda_X$  is the average number of type  $X$  points per unit area (Dixon, 2013). Note that the term “extra” is only necessary when  $X = Y$  to exclude the typical point itself from the count (provided the processes are jointly simple). In essence, this relates to counting the number of points of one type within a distance  $r$  of points of another type. Such a statistic can be computed easily, has a straightforward interpretation, and is easy to visualise (being a function of distance).

If we have additional points of type(s)  $Z = (Z_1, \dots, Z_p)$ , which we call covariate processes, the partial  $K$  function is informally

$$K_{XY \bullet Z}(r) = K_{XY}(r) - \frac{1}{\lambda_X} \mathbb{E} \left[ \begin{array}{l} \text{excess intensity of points of type } X \\ \text{linearly predicted from points of type } Z \\ \text{within distance } r \text{ of a typical point of type } Y \end{array} \right].$$

In other words, we take the usual  $K$  function and remove from it the clustering/repulsion which could be explained by linear prediction from  $Z$ , the covariate processes. The reason we do this linearly is because we can easily construct non-parametric estimators, without needing to specify a model *a priori*. This linear construction does have limitations: the resulting statistic is partial and not conditional (Baba et al., 2004). This means one cannot interpret the partial  $K$  function as detecting conditional orthogonality. However, the partial  $K$  function still provides a powerful tool for unpicking complicated dependence structures which may be present in the observed points patterns.

The main contributions of this paper are as follows. First, we introduce a family of partial functional statistics, which reduce to the classical point process equivalents when the covariate processes are independent of the processes of interest. Second, we provide reliable estimates for these quantities, including developing important debiasing steps which we show can have significant impact on the quality of the estimators. Third, we give detailed examples illustrating how these statistics work in a variety of cases designed to correspond to phenomena that are of interest in practice. Finally, we provide a clear interpretation of our novel statistics that can be thought of as taking the existing statistic and making an adjustment to account for the covariate processes, thus making it easier for practitioners to adopt. Therefore, this paper provides a new angle to analyse point pattern data, enabling us to extract new insights into the processes of interest.

## 2 Background

### 2.1 Point processes

Point processes are a type of stochastic process that model the random locations of points in some space, e.g.  $\mathbb{R}$  for temporal point processes or  $\mathbb{R}^2$  for spatial point processes. The material in this section can be found in standard textbooks on point processes, such as Møller and Waagepetersen (2003), Daley and Vere-Jones (2003) and Illian et al. (2008). Formally, a *point process* is a random measure  $N$  on  $\mathbb{R}^d$  taking values in the non-negative integers  $\mathbb{N}_0$ . For a Borel set  $B \in \mathcal{B}(\mathbb{R}^d)$ ,  $N(B)$  is the random number of points in  $B$ . The *support* of  $N$  is the set of point locations in  $\mathbb{R}^d$ . We say that a point process is *simple* if no two points occur in the same location almost surely (for all  $x \in \mathbb{R}^d$ ,  $N(\{x\}) \in \{0, 1\}$  a.s.), which is usually a natural assumption when modelling distinct locations. Such a framework provides a rigorous formalism to develop models for applications where point locations are the primary object of interest.

Multitype point processes generalize point processes to settings with multiple types of points. For example, say that we have three types,  $X$ ,  $Y$  and  $Z$ , then we can define multiple point processes  $N_X$ ,  $N_Y$  and  $N_Z$  to represent them. The *ground process* is the point process which contains all points of all types, and is defined as  $N = N_X + N_Y + N_Z$ . For notational convenience we use  $X$  to refer to the set of points of type  $X$ , and similarly for  $Y$  and  $Z$ . We assume that the ground process is simple, meaning that no two points of any type occur in the same location almost surely. Such multitype point processes enable us to model interactions between different types of points.

Throughout this manuscript, we assume the system of point processes is jointly *homogeneous*, meaning the joint distribution across process types is invariant under spatial translations (see Daley and Vere-Jones, 2007, for a formal definition). Say that we have three types of processes  $X$ ,  $Y$  and  $Z$ . As previously noted, the  $K$  function  $K_{XY}$  may be misleading if there is dependence between  $X$  and  $Y$  induced by  $Z$ , and this means  $K_{XY}$  not only requires that the spatial joint distribution of  $X$  and  $Y$  is homogeneous, but also conditionally on the locations of  $Z$ . Our partial  $K$  function relaxes this assumption to allow for certain forms of conditional mean inhomogeneity. We require only that the system  $(X, Y, Z)$  is jointly homogeneous, not that individual processes are conditionally homogeneous given others. This is a weaker requirement because processes can exhibit apparent spatial trends due to dependence on other processes, even if the system is homogeneous.

## 2.2 Summary statistics for point processes

There are many different summary statistics for point processes, see e.g. Illian et al. (2008) for an overview. For clarity of exposition, we will focus on point processes in two dimensional space (i.e.  $d = 2$ ), though the extension to general dimensions is straightforward, see Section S2.1. The first statistic of interest to us is the *intensity* of a point process. In general, the intensity measure is  $\Lambda_X(B) = \mathbb{E}[N_X(B)]$  for a Borel set  $B \in \mathcal{B}(\mathbb{R}^2)$ . However, when the process is homogeneous, the intensity measure has a constant density,  $\lambda_X$ , which we will call the intensity, and can be interpreted as the average number of points per unit area. We will assume that  $\lambda_X > 0$  for all processes considered here.

In order to introduce the remaining statistics, we first need to define the *second-order reduced moment measure* between the processes of type  $X$  and type  $Y$ , which for bounded  $B \in \mathcal{B}(\mathbb{R}^2)$  is

$$\check{M}_{XY}(B) = \mathbb{E} \left[ \int_{\mathbb{U}^2} N_X(B + y) N_Y(dy) \right],$$

where  $\mathbb{U}^2 = [0, 1]^2$  is the unit square (Daley and Vere-Jones, 2003). Then Ripley's *K function* is defined as

$$K_{XY}(r) = \lambda_X^{-1} \lambda_Y^{-1} \check{M}_{XY}(rS_0^2), \quad r \geq 0,$$

where  $S_0^2 = S^2 \setminus \{0\}$  and  $S^2$  is the unit ball in  $\mathbb{R}^2$ . If  $X = Y$  then this is called the *K function* of  $X$ , otherwise it is called the cross *K* function between  $X$  and  $Y$ . The *K* function can be interpreted as the expected number of points of type  $X$  within a distance  $r$  of a typical point of type  $Y$ , divided by the expected number of points of type  $X$  in a unit area (provided the processes are homogeneous).

Typically, the *K* function is transformed so that it is easier to interpret visually. A common transformation is the *L function* (Besag, 1977), which is

$$L_{XY}(r) = \sqrt{\frac{K_{XY}(r)}{\pi}}, \quad r \geq 0.$$

The benefits of this transformation are that  $L_{XY}(r) = r$  if the points of type  $X$  are independent of points of type  $Y$  (or if the process is Poisson when  $X = Y$ ), and the transformation is variance stabilising (Besag, 1977). Another common related statistic is the *pair correlation function*, which is defined as

$$g_{XY}(r) = \frac{K'_{XY}(r)}{2\pi r}, \quad r > 0.$$

The pair correlation function is one when the points of type  $X$  are independent of points of type  $Y$  (or when  $X = Y$  is a Poisson process).

A useful statistic for our purposes, which we will call the *C function*, is for  $r \geq 0$ ,  $C_{XY}(r) = \check{C}_{XY}(rS_0^2)$ , where  $\check{C}_{XY}(B) = \check{M}_{XY}(B) - \lambda_X \lambda_Y \ell(B)$  is the reduced covariance measure (for  $B \in \mathcal{B}(\mathbb{R}^2)$ ). The *C* function is easily related to the *K* function and pair correlation function by for all  $r > 0$

$$K_{XY}(r) = \frac{C_{XY}(r)}{\lambda_X \lambda_Y} + \pi r^2, \quad g_{XY}(r) = \frac{C'_{XY}(r)}{2\pi r \lambda_X \lambda_Y} + 1,$$

where the former equation holds also for  $r = 0$ . When the points of type  $X$  are independent of points of type  $Y$ , then  $C_{XY}(r) = 0$  for all  $r \geq 0$ . The *C* function is useful because it can easily be related to the spectral density function, which is

$$f_{XY}(k) = \int_{\mathbb{R}^2} e^{-2\pi i u \cdot k} \check{C}_{XY}(du), \quad k \in \mathbb{R}^2,$$

provided that  $\check{C}_{XY}$  is totally finite (Daley and Vere-Jones, 2003). For partial statistics, it is easiest to work with the spectral density function, and so transforming from the spectral density function to spatial statistics is a useful step. In particular, if  $f_{XY} - \check{M}_{XY}(\{0\}) \in L^1$  then

$$\begin{aligned} C_{XY}(r) &= \int_{\mathbb{R}^2} [f_{XY}(k) - \check{M}_{XY}(\{0\})] \frac{r}{\|k\|} J_1(2\pi \|k\| r) dk, & r \geq 0, \\ C'_{XY}(r) &= \int_{\mathbb{R}^2} [f_{XY}(k) - \check{M}_{XY}(\{0\})] 2\pi r J_0(2\pi \|k\| r) dk, & r \geq 0, \end{aligned}$$

where the derivation can be found in Section S2.3. If the processes  $X$  and  $Y$  are jointly simple, we have  $\check{M}_{XX}(\{0\}) = \lambda_X$  and  $\check{M}_{XY}(\{0\}) = 0$  when  $X \neq Y$ . In practice, Section 2.2 can be used to compute the pair correlation function, or we can use existing approaches to obtain an estimate from the estimated *K* function using smoothing splines, either directly from the *K* function or from some transformation, see Baddeley and Turner (2005) for details.

### 3 Partial $K$ function

#### 3.1 Comparison to existing methods

Partial statistics in the Fourier-domain are computationally efficient linear methods used to account for the influence of covariate processes. Such methods have been proposed for time series (Brillinger, 1972; Dahlhaus, 2000), random fields (Guinness et al., 2014), spatial point processes (Eckardt and Mateu, 2019) and combinations of point processes and random fields (Grainger et al., 2025). However, in many applications where spatial point patterns are recorded, the wavenumber-domain is unfamiliar to practitioners, and can be fundamentally harder to interpret. For example, while ocean waves are naturally understood as combinations of different frequency components (waves), the same wavenumber decomposition is less intuitive for analysing, say, tree locations in a forest.

For temporal point processes, Eichler et al. (2003) proposed a time-domain statistic based on transforming partial spectra back from the frequency domain. However, their approach has significant limitations for spatial applications. Their statistic is equivalent to a one-dimensional scaled version of the derivative of what we call the  $C$  function (see Section 2.2), which is not standard in the spatial point process literature, making it difficult to compare with existing methods and hindering adoption by practitioners.

Our proposed statistic resolves these issues by proposing a partial equivalent of the widely-used  $K$  function. The partial  $K$  function we develop is a direct generalization that reduces to exactly the usual  $K$  function when there is no influence from the covariate processes, enabling practitioners to interpret partial and non-partial statistics on the same scale using familiar methodology.

#### 3.2 Residual processes

We will usually refer to the process (typically  $X$ ) or pair of processes (typically  $X$  and  $Y$ ) which we are considering the interactions between as the *processes of interest*. The process(es) which we are accounting for (typically  $Z$ ), we call the *covariate processes*. One can account for any number of covariate processes, see Section S2.2 for the full details, but for clarity of exposition, we will consider the case where we have only one covariate process  $Z$ .

To have a notion of partial statistics, we first need to define linear prediction. Here, linear prediction means a convolution between the point process and a kernel signed measure designed to minimize the variance of the error whilst being unbiased. Let  $N_X^0(A) = N_X(A) - \lambda_X \ell(A)$  be the centred count measure and  $\mathcal{S}_{\mathbb{R}^2}$  be the set of totally finite signed measures on  $\mathbb{R}^2$ . More formally, we define the best linear prediction of  $X$  from  $Z$  as  $\Lambda_{X \bullet Z}(A) = \lambda_X \ell(A) + \Lambda_{X \bullet Z}^0(A)$  where

$$\Lambda_{X \bullet Z}^0(A) = \int_{\mathbb{R}^2} W_{X \bullet Z}(A - x) N_Z^0(dx), \quad A \in \mathcal{B}(\mathbb{R}^2),$$

and

$$W_{X \bullet Z} = \underset{W \in \mathcal{S}_{\mathbb{R}^2}}{\operatorname{argmin}} \operatorname{var} \left( N_X^0(\mathbb{U}^2) - \int_{\mathbb{R}^2} W(\mathbb{U}^2 - x) N_Z^0(dx) \right).$$

As discussed in Daley and Vere-Jones (2003), Chapter 8.5,  $\Lambda_{X \bullet Z}^0$  may not always be well-defined. However, this is still useful to provide interpretation for the proposed statistic, which does exist under mild assumptions. Assuming that for all  $k \in \mathbb{R}^2$ , the spectral matrix  $f(k)$  is invertible,  $W_{X \bullet Z}$  has Fourier transform

$$\tilde{w}_{X \bullet Z}(k) = \int_{\mathbb{R}^2} e^{-2\pi i u \cdot k} W_{X \bullet Z}(du) = f_{XZ}(k) f_{ZZ}(k)^{-1} \quad k \in \mathbb{R}^2.$$

The main motivation for using signed measures,  $W$ , for the prediction kernel is that in some situations we can predict point locations exactly. For example, say that we have a process  $Z$  and we make  $X$  by taking all the points in  $Z$  and applying the same deterministic shift,  $s$ , to all points, so that  $x = z + s$  (or  $N_X(A) = N_Z(A - s)$ ). Then we obtain  $\check{C}_{XZ}(B) = \check{C}_{ZZ}(B - s)$ , so  $f_{XZ}(k) = e^{-2\pi i k \cdot s} f_{ZZ}(k)$  and therefore  $\tilde{w}_{X \bullet Z}(k) = e^{-2\pi i k \cdot s}$ . This is the Fourier transform of the Dirac measure centred at  $s$ ,  $\delta_s(A) = \mathbb{1}_A(s)$ . Furthermore, for bounded  $A \in \mathcal{B}(\mathbb{R}^2)$

$$\begin{aligned} \Lambda_{X \bullet Z}(A) &= \lambda_X \ell(A) + \int_{\mathbb{R}^2} \delta_s(A - z) N_Z^0(dz) \\ &= \int_{\mathbb{R}^2} \delta_z(A - s) N_Z(dz) = N_Z(A - s) = N_X(A). \end{aligned}$$

So, as expected, we can perfectly predict the locations of type  $Z$  from type  $X$  in this setting. While this is an unrealistic and idealised case, it demonstrates that the construction behaves correctly in an extreme scenario. However, usually  $W_{X \bullet Z}$  will have a density, which we denote by  $w_{X \bullet Z}$ . In this case,  $\Lambda_{X \bullet Z}$  also has a density

$$\begin{aligned}\lambda_{X \bullet Z}(u) &= \lambda_X + \int_{\mathbb{R}^2} w_{X \bullet Z}(u - z) N_Z^0(dz) \\ &= \lambda_X - \lambda_Z \int_{\mathbb{R}^2} w_{X \bullet Z}(u) du + \sum_{z \in Z} w_{X \bullet Z}(u - z),\end{aligned}$$

for all  $u \in \mathbb{R}^2$ . So we can see  $\lambda_{X \bullet Z}(u)$  as being a linear prediction of the intensity of  $X$  at a point  $u$  in space made by putting a kernel on every point of type  $Z$  plus some intercept term. When  $X$  arises from a Neyman-Scott process with clusters centred at  $Z$ , we have  $\lambda_{X \bullet Z}(u) = \sum_{z \in Z} w_{X \bullet Z}(u - z)$ , for all  $u \in \mathbb{R}^2$ . When  $X$  and  $Z$  are independent we have  $\lambda_{X \bullet Z}(u) = \lambda_X$  for all  $u \in \mathbb{R}^2$ .

In any case, we define the residual process as

$$\epsilon_{X \bullet Z}(A) = N_X(A) - \Lambda_{X \bullet Z}^0(A), \quad A \in \mathcal{B}(\mathbb{R}^2).$$

Note that the residual process is defined in terms of  $N_X$ , and  $\Lambda_{X \bullet Z}^0$  (and not  $N_X^0$ ). This is deliberate, as it means  $\epsilon_{X \bullet Z}$  has a constant intensity of  $\lambda_X$  and not zero, allowing us to define direct analogues of the usual point process statistics. Even if  $\Lambda_{X \bullet Z}^0$  is well-defined, the residual process still may not be well-defined. This is because, in principle, for unbounded  $A$ ,  $N_X$  and  $\Lambda_{X \bullet Z}^0$  may both be infinite. However, again this is still useful to provide interpretation for the proposed statistics. It should be noted, these residuals are different from the residuals used as diagnostics for point process modelling (Baddeley et al., 2005, 2008), as we are not subtracting the conditional intensity of a process under a model, but rather a linear combination of the other processes.

### 3.3 Partial statistics

Having defined residual processes, we can now construct partial versions of standard point process statistics. We define partial statistics to be equivalent to their usual statistics, but from the residual processes. For notational convenience, we write  $\lambda_{X \bullet Z} = \lambda_{\epsilon_{X \bullet Z}}$ ,  $K_{XY \bullet Z}(r) = K_{\epsilon_{X \bullet Z}, \epsilon_{Y \bullet Z}}(r)$ , and so on. In particular

$$K_{XY \bullet Z}(r) = \lambda_X^{-1} \lambda_Y^{-1} \mathbb{E} \left[ \int_{\mathbb{U}^2} \epsilon_{X \bullet Z}(r S_0^2) \epsilon_{Y \bullet Z}(dy) \right].$$

However, since the residual processes are not necessarily positive (from Section 3.2), the partial  $K$  function does not need to be positive nor increasing. If the partial  $K$  function is negative, then the partial  $L$  function is not real-valued, as the  $L$  function square roots the  $K$  function. Therefore, we will replace the  $L$  function with a signed version, so that instead

$$L_{XY \bullet Z}(r) = \text{sgn}(K_{XY \bullet Z}(r)) \sqrt{\frac{|K_{XY \bullet Z}(r)|}{\pi}}, \quad r \geq 0,$$

where  $\text{sgn}$  is the sign function. For the  $K$  function, the signed  $L$  function is the usual  $L$  function, as the  $K$  function is always non-negative.

In order to compute these various statistics, we exploit the relationship between the partial  $K$  function and the partial spectral density function, a quantity which we can compute from the spectral density function of the underlying processes. Using analogous arguments to the time series case (Brillinger, 1974, Theorem 8.3.1),

$$f_{XY \bullet Z}(k) = f_{\epsilon_{X \bullet Z}, \epsilon_{Y \bullet Z}}(k) = f_{XY}(k) - f_{XZ}(k) f_{ZZ}(k)^{-1} f_{ZY}(k),$$

for all  $k \in \mathbb{R}^2$ , see Proposition S1 for details. Sections 3.2 and 3.3 continue to hold when there are multiple  $Z$  processes, but now  $f_{XZ}$  is a row vector,  $f_{ZZ}(k)$  is a matrix and so on.

It is important that we can continue to use the inversion results in Section 2.2. In order to do this, we need to be able to describe the atom at zero in  $\check{M}_{XX \bullet Z}$ . When  $\Lambda_{X \bullet Z}$  admits a density, we have  $\check{M}_{XX \bullet Z}(\{0\}) = \lambda_X$  and  $\check{M}_{XY \bullet Z}(\{0\}) = 0$  when  $X \neq Y$ . In general, this does not necessarily hold, even if  $X, Y, Z$  are jointly simple.<sup>5</sup> However, in practice the atom usually will be of this form, and so we assume this from now on.

<sup>5</sup>A simple example is when  $Z$  is obtained by applying a deterministic non-zero shift to  $X$ . In this case, the residual process is almost surely  $\lambda_X$  times the Lebesgue measure, so the reduced covariance measure of the residual process is the zero measure, so that  $\check{M}_{XX \bullet Z}(\{0\}) = 0$ . This is, however, somewhat pathological.

### 3.4 Interpretation

The usual  $K$  function has a clean interpretation in terms of typical points, so that  $\lambda_X K_{XY}(r)$  is the expected number of points of type  $X$  within a distance  $r$  of a typical point of type  $Y$ . This interpretation arises from Palm theory (see e.g. Møller and Waagepetersen, 2003, Section C.2), which allows us to think about the distribution of a point process conditional on a point being at a certain location (Illian et al., 2008, Section 4.1). In fact, we can construct a similar interpretation for the partial  $K$  function by performing some rearrangement. In particular, one can see that

$$K_{XY \bullet Z}(r) = K_{\epsilon_{X \bullet Z}, \epsilon_{Y \bullet Z}}(r) = K_{\epsilon_{X \bullet Z}, Y}(r).$$

Intuitively this is because the difference between  $K_{XY \bullet Z}(r)$  and  $K_{\epsilon_{X \bullet Z}, Y}(r)$  is

$$\lambda_X^{-1} \lambda_Y^{-1} \mathbb{E} \left[ \int_{\mathbb{U}^2} \epsilon_{X \bullet Z}(y + rS_0^2) \Lambda_{Y \bullet Z}^0(dy) \right]$$

which is essentially the correlation between a residual and one of the predictors, and so should be zero (see Proposition S3).

Given this, we now have an expression which only integrates against points in  $Y$ , meaning we can have a typical point interpretation as

$$\begin{aligned} \lambda_X K_{XY \bullet Z}(r) &= \lambda_Y^{-1} \mathbb{E} \left[ \int_{\mathbb{U}^2} \epsilon_{X \bullet Z}(rS_0^2) N_Y(dy) \right] \\ &= \mathbb{E}_0^Y [\epsilon_{X \bullet Z}(y + rS_0^2)] \\ &= \lambda_X K_{XY}(r) - \mathbb{E}_0^Y [\Lambda_{X \bullet Z}^0(rS_0^2)] \end{aligned}$$

where  $\mathbb{E}_0^Y$  denotes the expectation conditional on there being a point of type  $Y$  at the origin. Therefore, we can interpret  $\lambda_X K_{XY \bullet Z}(r)$  as the expected number of points of type  $X$  within a distance  $r$  of a typical point of type  $Y$  minus the  $Z$ -based linear prediction of the excess of  $X$  within a distance  $r$  of a typical point of type  $Y$ . Here the excess linear prediction is the linear prediction minus the intensity  $\lambda_X$ , so that it has mean zero, and in particular can be negative. Notice that  $\Lambda_{X \bullet Z}^0$  is random, and its mean is zero. However, its conditional mean on a point of type  $Y$  being at the origin, the last term in Section 3.4, is not necessarily zero.

### 3.5 Limitations

It is important to be aware of the limitations of any proposed statistics. For the statistics proposed here, the first limitation is that we are considering only second-order properties of the processes. In the case of the usual  $K$  function, Baddeley and Silverman (1984) provided a nice example of a univariate process whose  $K$  function is identical to that of a Poisson process, but which is certainly not a Poisson process. This limitation extends also to the partial statistics proposed here.

For partial statistics, there is an additional, stronger, limitation. For random vectors, Baba et al. (2004) characterise the difference between partial and conditional correlation, which are not necessarily equal in the non-Gaussian setting. Similarly, if the  $K_{XY}(r) \neq \pi r^2$  then  $X$  and  $Y$  are dependent. However, it is possible to have  $K_{XY \bullet Z}(r) \neq \pi r^2$ , even when  $X$  and  $Y$  are conditionally independent given  $Z$ . This is because the partial  $K$  function only accounts for linear trends in conditional means. It has been claimed in the literature that partial statistics can provide tests of conditional orthogonality/independence (Eckardt and Mateu, 2019). Unfortunately, this is not true, as can be seen from the example below, and it is important that practitioners are aware of this limitation. Nonetheless, partial statistics can still be useful to account for covariate processes, especially for exploratory analysis.

Let  $N_Z$  be a homogeneous Poisson process with intensity  $\lambda_Z > 0$  on  $\mathbb{R}^d$ . Now let  $\Lambda(u) = [\int_{\mathbb{R}^d} g(u - x) N_Z(dx)]^2$  for some kernel  $g : \mathbb{R}^d \rightarrow [0, \infty)$ . Then let  $N_X$  and  $N_Y$  be Cox processes driven by  $\Lambda$  but conditionally independent of each other given  $\Lambda$ . Then the partial spectra between  $X$  and  $Y$  accounting for  $Z$  is

$$f_{XY \bullet Z}(k) = 2\lambda_Z^2 [|G|^2 * |G|^2](k), \quad k \in \mathbb{R}^d,$$

where  $G$  is the Fourier transform of  $g$ ,  $|G|^2$  is its elementwise magnitude square and  $*$  denotes convolution (see Section S2.6). The partial spectra  $f_{XY \bullet Z}(k)$  is therefore not identically zero. This contradicts the claim that tests for zero partial spectra (or partial coherence) can be used as tests of conditional orthogonality, as here the partial spectra is not zero, despite the processes being conditionally independent (and thus orthogonal).

## 4 Examples

We demonstrate the differences between the  $K$  function and the partial  $K$  function with simulated examples. The first collection of examples show how partial statistics can already be useful for bivariate systems, and then the following examples explore partial statistics for trivariate systems.

For the sake of illustration, we compare both the  $L$  function and partial  $L$  function to null confidence intervals for the  $L$  function. It would be preferable to have two different null intervals, however, resampling for these partial statistics is difficult, and remains an open problem (see the discussion in Section S3). Whilst we focus on the  $L$  function here, similar results for the pair correlation function can be found in Section S6.2, though it should be noted that estimates of the pair correlation function are less reliable than those for the  $K$  function (as one would expect because the  $K$  function is cumulative but the pair correlation function is a density). The details on the specific parameter setups for each model can be found in Section S5.

### 4.1 Examples for intraprocess statistics

Consider a simple predator prey like system, where there is some prey species whose locations we observe and then a predator species which clusters around them. We could reasonably consider three scenarios:

- Independent: the predators do not interact with each other.
- Packs: the predators hunt in packs.
- Solitary: the predators are solitary.

In order to generate such a process, consider the following model. Take the prey species,  $Y$ , to be located like a Poisson process with constant intensity  $\lambda_Y$  (e.g. centroid of a prey animal group). Then generate an intermediary point process  $X_0$  by placing clusters at every location of type  $Y$  with a random number of predators at random offsets from the prey. In this case, we will have  $\text{Poisson}(\eta_{X_0})$  points and the offset of a point from the parent will be  $\text{Normal}(0, \sigma_{X_0}^2 I)$ , so the offspring arise from the modified Thomas process (Thomas, 1949). To generate the predator process in the first scenario (independent), we simply set  $X = X_0$ . To generate the predator process in the second situation (packs), we repeat this process to generate  $X$  by placing clusters around points of type  $X_0$  in the same manner with parameters  $\eta_X$  and  $\sigma_X^2$ , retaining only types  $X$  and  $Y$  points. To generate the predator process in the final scenario (solitary), we take the points of type  $X_0$  and assign to each point a random mark in  $[0, 1]$ . Then any point within a distance  $r_X$  of another point of type  $X_0$  with a higher mark than itself dies with probability  $1 - p_X$ , so that  $p_X$  is the probability of a point surviving if it is within the influence of a higher-marked neighbour. The points  $X$  are then set to be the survivors. The  $X$  pattern is marginally a generalisation of a Matérn hard-core process (though not quite the same as those in (Teichmann et al., 2013)).

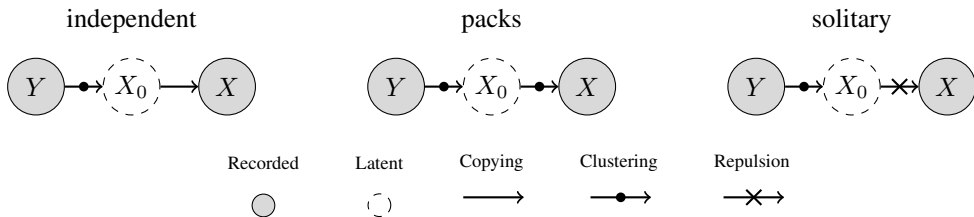


Figure 1: Schematic of the predator prey system with three different interaction types.

Examples of such processes are shown in Fig. 2 as insets, with estimated  $L$  and partial  $L$  functions for the  $X$  process with itself,  $\hat{L}_{XX}$  and  $\hat{L}_{XX \bullet Y}$  respectively, shown as the main plot. We see in all three cases, the usual  $L$  function is positive, indicating that there is a clustering behaviour. However, when we consider the partial  $L$  function, we see that in the first case, the partial  $L$  function is very close to the independence line  $L(r) = r$ , indicating that there is no additional clustering or repulsion after accounting for the prey process. In the second case, we see that the partial  $L$  function is above the line  $L(r) = r$ , indicating that there is additional clustering among the predators after accounting for the prey process. In the third case, we see that the partial  $L$  function is below the line  $L(r) = r$ , indicating that there is repulsion among the predators after accounting for the prey process. This is exactly what we would expect given the choice of examples.

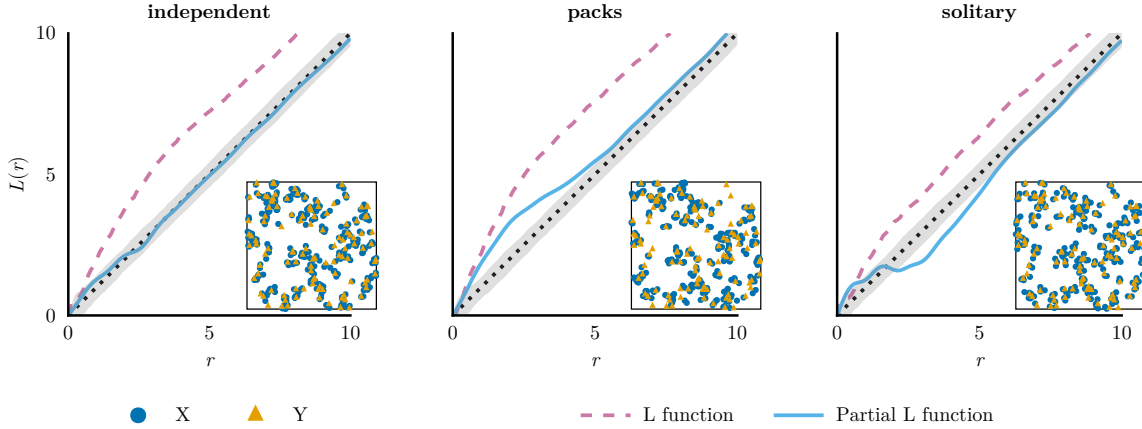


Figure 2: Example of a predator-prey system with three different interaction types. The main plots are the  $L$  function and partial  $L$  function between the predator process ( $X$ ) in the latter case accounting for the prey process ( $Y$ ). The left column shows the first scenario, where the predators do not interact with each other. The middle column shows the second scenario, where the predators hunt in packs. The right column shows the third scenario, where the predators do not like to be near each other. The envelopes are 95% confidence envelopes for the  $L$  function under independence, using the MAD envelopes proposed by Myllymäki et al. (2017).

#### 4.2 Examples for interprocess statistics

Another interesting scenario to consider is a three process system, where we now have processes  $X$ ,  $Y$  and  $Z$ . We will assume that the process  $Z$  is again Poisson, and that the process  $Y$  is generated from  $Z$  in the manner of the first example described in the previous section. We then generate  $X$  by one of three mechanisms:

- Independent offspring:  $X$  and  $Y$  independently cluster around  $Z$ .
- Co-operative offspring:  $X$  is generated by placing clusters around points of type  $Y$ .
- Antagonistic offspring:  $X$  is generated from  $Z$  independently of  $Y$ , then thinned by points of type  $Y$ .

Realisations of such processes, along with their estimated  $L$  and partial  $L$  functions are shown in Fig. 4. We can see that the usual  $L$  functions always indicate cross clustering, in all scenarios for all processes other than between  $X$  and  $Y$  in the agnostic offspring case (where the  $L$  function indicates no interaction, but we expect repulsion). However, the partial equivalents successfully recover the underlying structure. In particular, in the first column ( $X$  vs  $Y$  accounting for  $Z$ ) we see no clustering, clustering and repulsion respectively. This is as expected, as in the first case the  $X$  and  $Y$  processes independently cluster around  $Z$ , in the second  $X$  clusters around  $Y$  and in the third  $X$  is thinned by  $Y$ . In the second column ( $X$  vs  $Z$  accounting for  $Y$ ), we see clustering, no behaviour and clustering again. Again, this correctly reflects the underlying dependence structure because in the first and last cases, the  $X$  process does cluster around the  $Z$  process (in the latter case it is then repulsed by  $Y$ , but some clustering remains), but in the middle case,  $X$  directly depends on  $Y$  and not  $Z$ , so after accounting for this we have no structure left, as expected. In the final column ( $Y$  with  $Z$  accounting for  $X$ ), we see clustering in all three cases. Again this is as expected because  $Y$  is always generated to be clustered around  $Z$  and then not modified. Clearly at least in this example, the partial  $L$  function provides a useful additional tool to explore interactions in such point pattern datasets.

#### 4.3 Superpositions of independent processes

Another interesting case is when we have superpositions of independent processes. In particular, say that  $X$  and  $Y$  are independent of the covariate process  $Z$ . In this case, the partial  $K$  function is identical to the usual  $K$  function, i.e.  $K_{XY \bullet Z} = K_{XY}$ . Furthermore, this includes the intra process statistics too, i.e.  $K_{XX \bullet Z} = K_{XX}$ . This holds because the prediction process  $\Lambda_{X \bullet Z}$  is zero almost surely, as  $f_{XY} = 0$ .

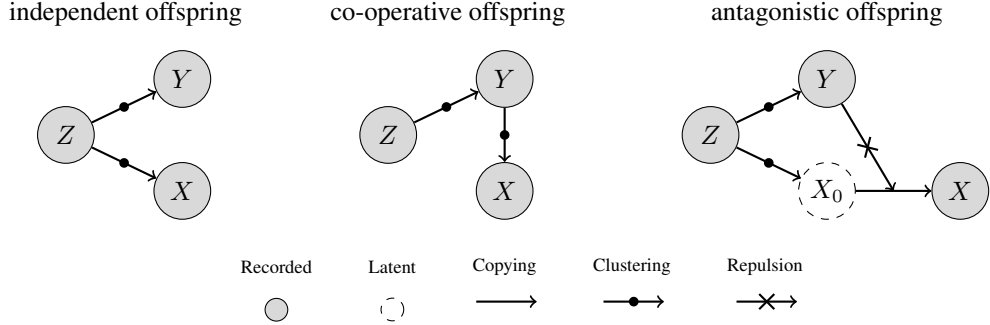


Figure 3: Schematic of the trivariate system with three different interaction types.

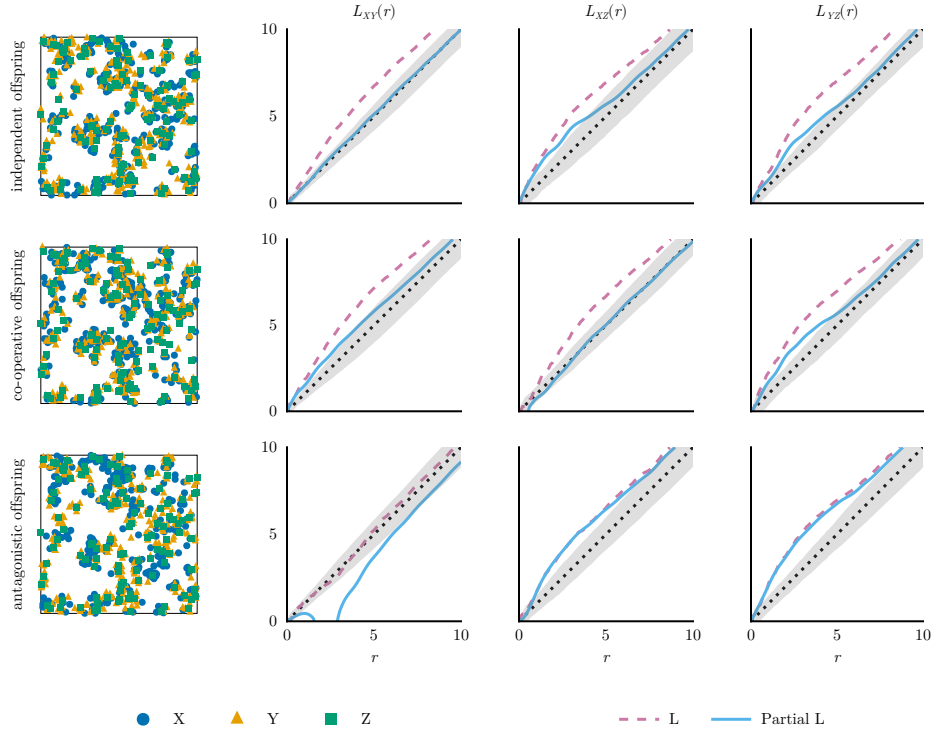


Figure 4: Example of a trivariate system with three different interaction types. The first column shows example processes, the second column shows the  $L$  function and partial  $L$  function between process  $X$  and process  $Y$  (possibly accounting for process  $Z$ ), the third column shows interactions between  $X$  and  $Z$  (accounting for  $Y$ ) and the final column shows interactions between  $Y$  and  $Z$  (accounting for  $X$ ).

## 5 Estimation

### 5.1 Spectral estimation

We assume that we observe data on some bounded observational region  $\mathcal{R}$ . To construct estimators for the partial  $K$  function, first need estimators of the spectral density function, and then the partial spectral density function. We will use the multitaper method (Thomson, 1982; Grainger et al., 2025) as this allows us to construct reliable estimators of the spectral density function from observations on arbitrary domains. Briefly, given a family of tapers,  $h_1, \dots, h_M$  supported on a subset of  $\mathcal{R}$ , we construct tapered periodograms

$$I_{XY;m}(k) = J_{X;m}(k) \overline{J_{Y;m}(k)} \quad k \in \mathbb{R}^2,$$

where

$$J_{X;m}(k) = \int_{\mathcal{R}} h_m(x) e^{-2\pi i x \cdot k} N_X(dx) - \hat{\lambda}_X H_m(k) \quad k \in \mathbb{R}^2,$$

with  $H_m(k)$  being the Fourier transform of the taper  $h_m$  at wavenumber  $k$ . Tapers are constructed either by interpolated Slepian tapers (on irregular domains) or by taking outer products of the minimum bias tapers (on regular domains), see Grainger et al. (2025) for details. The multitaper periodogram is subsequently defined as

$$\hat{f}_{XY}(k) = \frac{1}{M} \sum_{m=1}^M I_{XY;m}(k) \quad k \in \mathbb{R}^2.$$

This provides a reliable estimator of the spectral density function, whose properties are well understood (see e.g., Thomson, 1982; Walden, 2000; Grainger et al., 2025).

### 5.2 Basic estimator

In order to estimate the (partial)  $K$  function, we first estimate the (partial)  $C$  function and then use a discretization of Section 2.2. This technique can be used to estimate both the usual  $K$  function and the partial  $K$  function. We therefore describe it in terms of the usual case, but the (simple) partial case is a plug in of the partial spectral density function estimate (see Section 5.3 for additional debiasing).

In order to use Section 2.2, we need to discretize and truncate the integral. We do this by considering a finite set of wavenumbers  $\Omega \subset \mathbb{R}^2$  and then approximating the integral by a Riemann sum. In particular, let  $k^{\max} \in (0, \infty)^2$  be the maximum wavenumber and  $k^\Delta \in (0, \infty)^2$  be the spacing between wavenumbers in each dimension. Then  $\Omega = (k^{\max} \circ [-1, 1]^2) \cap (k^\Delta \circ \mathbb{Z}^2)$ .<sup>6</sup> We construct the estimator for  $C$  by

$$\hat{C}_{XY}(r) = k_1^\Delta k_2^\Delta \sum_{k \in \Omega} \left[ \hat{f}_{XY}(k) - \hat{\lambda}_X \delta_{X,Y} \right] \frac{r}{\|k\|} J_1(2\pi\|k\|r) \quad r \geq 0.$$

In general, the term  $\hat{\lambda}_X \delta_{X,Y}$  should be an estimator of  $\check{M}_{XY}(\{0\})$ , which is  $\lambda_X \delta_{X,Y}$  for a simple point process, but takes a different form for a marked point process for example, i.e. it is not the first moment of a random measure in general (Daley and Vere-Jones, 2003).

### 5.3 Debiasing

To obtain an estimate of the partial  $K$  function, we replace the estimated spectral density function with its partial counterpart. The naive estimator is a plug in, so that

$$\hat{f}_{XY \bullet Z}(k) = \hat{f}_{XY}(k) - \hat{f}_{XZ}(k) \hat{f}_{ZZ}(k)^{-1} \hat{f}_{ZY}(k) \quad k \in \mathbb{R}^2.$$

However, even if we have unbiased estimates of the spectral density function, Section 5.3 is a biased estimator of the partial spectra, and this bias can result in substantial bias for the  $K$  function.

In particular, consider the function which maps spectral density matrix functions to their partial equivalent

$$F_{XY \bullet Z}[f] = f_{XY} - f_{XZ} f_{ZZ}^{-1} f_{ZY}$$

<sup>6</sup>In practice, the output wavenumber grid corresponds to an FFT, and thus takes a specific form, but this is not important for the exposition here.

where  $f_{ZZ}^{-1}$  refers to pointwise matrix inversion (not the inverse of the function  $f_{ZZ}$ ). Then given some regularity conditions, for fixed  $M$ ,  $P$ , and growing domain, the plug in estimator satisfies

$$\mathbb{E} \left[ F_{XY \bullet Z}[\hat{f}] \right] = \left( 1 - \frac{P_Z}{M} \right) F_{XY \bullet Z}[f] + o(1)$$

where  $P_Z$  is the number of processes in  $Z$  and  $M$  is the number of tapers used to construct  $\hat{f}$  (see Theorem S1). Therefore, we can obtain an improved estimate by setting

$$\hat{f}_{XY \bullet Z} = \left( \frac{M}{M - P_Z} \right) F_{XY \bullet Z}[\hat{f}].$$

This is similar to the bias corrections required for estimating partial coherence (Medkour et al., 2009), though here we are directly interested in the partial spectra, not the partial coherence as is typically the case in other applications. Recall that we already require more tapers than processes, and therefore  $M > P_Z$ . When we compute partial  $L$  functions, we perform another non-linear transformation, which can warp this bias in unusual ways especially for short distances, which results in bias that is not just a percentage reduction, but which looks like a meaningful feature. A specific example of this phenomena is given in Section S6.3. The debiasing we propose resolves this problem, and removes such spurious features.

#### 5.4 Pre rotational averaging

So far, we have constructed our estimator by making direct use of Section 2.2 and plugging in our (debiased) estimate of the partial spectra. However, an alternative approach would be to first construct a rotationally averaged spectral estimate, and then compute a one-dimensional transform. The rational for this approach is, first, that we can reduce the number of evaluations of the Bessel functions, which are expensive. Second, because Bessel functions oscillate, the quality of the integral approximation can be poor if we cannot discretize enough. This can be tricky, because for small radii, we need to use many wavenumbers before the Bessel function gets small, but for large radii, we need a fine grid to capture their oscillatory behaviour. Therefore, a useful, faster and more stable alternative may be derived by considering

$$\begin{aligned} \hat{C}_{XY}(r) &= \sum_{\kappa \in \bar{\Omega}} \hat{f}_{XY}^{(rot)}(\kappa) \int_{\mathbb{R}^2} \mathbb{1}_{(\kappa - \frac{s}{2}, \kappa + \frac{\kappa^\Delta}{2}]}(\|k\|) \frac{r}{\|k\|} J_1(2\pi\|k\|r) dk \\ &= \sum_{\kappa \in \bar{\Omega}} \hat{f}_{XY}^{(rot)}(\kappa) 2\pi r \int_{\kappa - s/2}^{\kappa + s/2} J_1(2\pi x r) dx \\ &= \sum_{\kappa \in \bar{\Omega}} \hat{f}_{XY}^{(rot)}(\kappa) [J_0(2\pi r(\kappa - \kappa^\Delta/2)) - J_0(2\pi r(\kappa + \kappa^\Delta/2))] \end{aligned}$$

where  $\bar{\Omega} = (\kappa^\Delta/2 + \kappa^\Delta \mathbb{Z}) \cap [0, \kappa^{\max}]$  is a one dimensional vector of radial wavenumbers spaced  $\kappa^\Delta > 0$  apart so that the first radial wavenumber considered is bigger than  $\kappa^\Delta/2$ . The equivalent form for the  $d$ -dimensional case is given in Section S2.1.2. Notice that in Section 5.4, we are approximating the integral with the analytical integral assuming that  $\hat{f}_{XY}^{(rot)}$  is piecewise constant, and not with a Riemann sum. This results in greater stability, as the underlying spectra is often reasonable smooth relative to the weighted Bessel function it is integrated against.

#### 5.5 Hyperparameter selection

In order to estimate the partial  $K$  function, we need to select appropriate hyperparameters, namely, the number of tapers  $M$ , the highest wavenumber  $k^{\max}$ , and the spacing  $k^\Delta$ . The number of tapers,  $M$ , needs to be at least the number of processes,  $P$ , i.e.  $M \geq P$ , because otherwise we will not be able to invert the spectral matrix (Walden, 2000). Generally, since we aggregate to compute the partial  $K$  function, we do not need the tapers for variance reduction as much as we would if we were interested in estimating the partial spectra. Increasing the number of tapers corresponds to smoothing over a larger bandwidth in wavenumber, which will introduce bias. One simple option for selecting  $k^\Delta$  is to use  $1 \oslash L$  where  $L$  is the vector of side lengths of the bounding box of  $\mathcal{R}$  and  $\oslash$  denotes elementwise division. To select  $k^{\max}$ , we can either look at pilot estimates of the spectral density function, or use an iterative scheme where we repeatedly increase  $k^{\max}$  until we see a small change in the resultant  $K$  function. Another useful diagnostic check is to compare the  $K$  function estimated using standard methods to the  $K$  function (not partial) estimated from the spectral density function, which we would expect to be similar. In Section S6.4, we show in simulations that this spectral approach to estimating the  $L$  function is competitive with the standard border correction methods typically used when computing the usual  $L$  function.

The additional parameters in the pre rotational averaging approach are the radial wavenumber spacing  $\kappa^\Delta$  and maximum radial wavenumber  $\kappa^{\max}$ . One choice is to relate them to the previous parameters by  $\kappa^{\max} = \min_j k_j^{\max}$  and  $\kappa^\Delta = \min_j k_j^\Delta$ . The final choice is the form of rotational averaging to use. In particular, we use

$$\hat{f}_{XY}^{(rot)}(\kappa) = \frac{\sum_{k \in \Omega} f_{XY}(k) W_b(\|k\| - \kappa)}{\sum_{k \in \Omega} W_b(\|k\| - \kappa)}$$

where  $W_b(x) = W(x/b)/b$  in general. Typically, we use  $W(x) = \mathbb{1}_{[-1/2, 1/2]}(x)$ , and set  $b = 2 \max_j k_j^\Delta$  so that the averaging window always contains at least one wavenumber. We do not need the kernel smoothing for variance reduction here, and so the choice is not particularly important.

## 5.6 Computational complexity

The computational complexity of the estimation procedure is competitive with standard methods for estimating the  $K$  function. In particular, say that  $n$  is the total number of points,  $P$  is the number of processes,  $M$  is the number of tapers and  $R$  is the number of spatial distances at which we want to evaluate the  $K$  function. Then the complexity of computing the multitaper periodogram is  $O(PMn \log(n))$ , the complexity of computing the partial spectral density function is  $O(P^3|\Omega|)$  where  $|\Omega|$  is the number of wavenumbers considered, and the complexity of computing the  $K$  function from the spectral density function is  $O(R|\Omega|)$ . If we use a fixed highest wavenumber and the spacing rule proposed above, then  $|\Omega|$  scales as  $O(n)$  (as  $n$  scales like the region size). Therefore, the overall complexity is  $O(PMn \log(n) + P^3n + Rn)$ . The standard approaches for computing the  $K$  function have complexity  $O(P^2n^2)$ , and so for large  $n$  and fixed  $P$ , our approach is faster.

## 6 Accounting for covariates and long scale phenomena

In many applications, it is also important to be able to account for covariates. The partial  $K$  function developed here can be readily extended to add covariate effects by simply including them as covariate processes. In particular, say that we also observe some random fields  $W_1, \dots, W_Q$  over the same region as our point processes. We can treat these random fields as additional processes in our system. Then, we can estimate joint spectra using the methodology proposed by Grainger et al. (2025), and transform the resultant partial spectra back into space as described here. All of the additional results regarding bias effects translate exactly, with the slight caveat that there are some effects of sampling if the random fields are observed on a grid that is not sufficiently fine.

In particular, the spacing of the grid imposes a highest wavenumber for which we can estimate the spectra of the covariate process. If we needed to compute the whole spectral matrix beyond this point, e.g. because the point process spectra had useful information beyond this wavenumber, we would need to make a decision on how to handle the random field. The simplest option is to interpolate the covariate onto a grid that is sufficiently fine to capture all the wavenumbers of interest. Another alternative is for wavenumbers outside the Nyquist box of the covariate, we can compute the partial spectra of the processes not including the covariate, and then add those rows and columns back in as zeros. This would correspond to assuming the spectra of the covariate was zero in this range. A simulated example of such a system comparing the partial  $K$  function and inhomogeneous  $K$  function is shown in Section S6.1.

## 7 Exploratory Analysis of Lansing Woods data

We illustrate this technique on the Lansing Woods data (Gerrard, 1969). This canonical dataset consists of the locations of trees present in a forest plot in Lansing Woods, Michigan, USA. There are five named species of tree present, as well as a miscellaneous category. We account for the miscellaneous category as a covariate process, but do not consider it for analysis as it is hard to interpret biologically (being an aggregate of multiple rare species). The data has been widely studied in the spatial statistics literature, see Baddeley et al. (2015) for references. The data is available standardised to the unit square in the `spatstat` R package (Baddeley et al., 2015). The top row of Fig. 5 shows the locations of the six different tree species present in the Lansing woods dataset (with one of the species being miscellaneous).

The bottom row of Fig. 5 shows the estimated marginal  $L$  functions and partial  $L$  functions for each species with itself, accounting for all other species. When comparing the two, we see that the marginal  $L$  functions indicate more clustering behaviour than the partial  $L$  functions. This is not surprising as we would expect to see some of the clustering behaviour being explained by interactions with other species (Murrell, 2010). Figure 6 shows the cross  $L$  functions and partial  $L$  functions between different species, again accounting for all other species. Here we again see that some of the clustering behaviour seen in the cross  $L$  functions is explained away by the other species. In some cases, the interaction essentially disappears, even slightly changing sign (e.g. Black Oak vs Hickory). This general behaviour is expected, as the partial

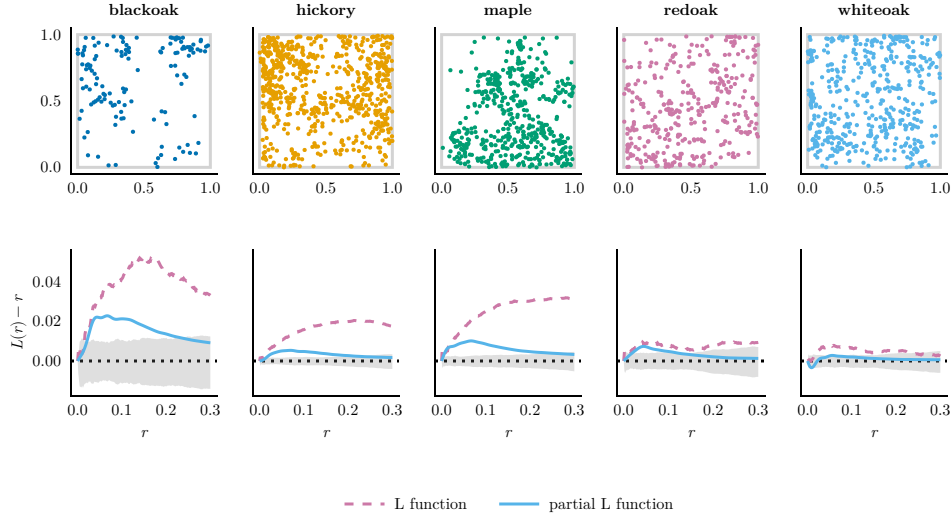


Figure 5: Lansing woods data (top row) and the estimated  $L$  and partial  $L$  functions within processes (bottom row).

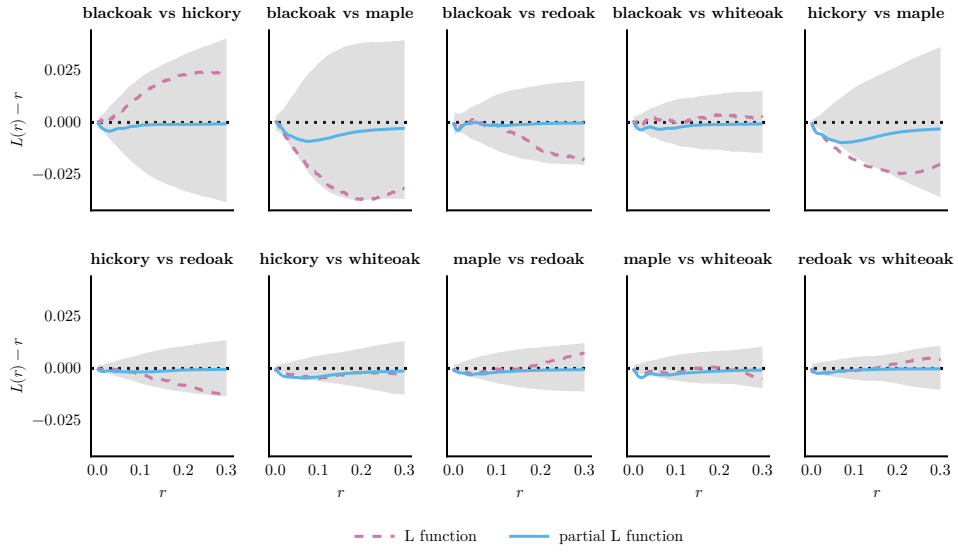


Figure 6: Estimated cross  $L$  and partial  $L$  functions for the Lansing woods data.

$L$  function has accounted for some of the other processes, meaning that some of the observed clustering/repulsion has been removed by accounting for the covariate processes. The resulting “sparser” representation of the dependence structure between and within the processes can then be used to highlight the more important interactions.

## 8 Discussion

In this paper, we proposed the partial  $K$  function, an extension of the usual  $K$  function which accounts for some effects of the other processes involved in the system of interest. The partial  $K$  function is easy to compute, non-parametric, and we have boundary corrections for non-rectangular domains. Furthermore, we can easily include covariate information by treating them as random fields, which can be incorporated into the same methodology. This technique provides

a powerful additional tool for understanding the interactions between multiple point processes, complementing the existing approaches.

However, as with any statistical technique, there are limitations. Internally, the partial  $K$  function is based on linear prediction, which is not particularly natural for non-negative quantities (such as random measures). As we observe more processes, obtaining well-conditioned estimates of the coherence and partial coherence, and thus estimating the partial  $K$  becomes challenging (see e.g. Walden (2000)). This remains an outstanding problem. Additionally, it is important to develop null resampling methods, which is a difficult problem for any point process statistic. Furthermore, our current estimator uses anisotropic spectral estimates, meaning that it can be interpreted as an isotropic summary of potentially anisotropic processes. If we are confident that processes are isotropic, then it may be better to first average spectral estimates rotationally before computing partial spectra and partial  $K$  functions.

In summary, the partial  $K$  function (and other derived quantities) provide useful additional tools for exploring point pattern data. By accounting for the other kinds of points present in an observational area, we are able to uncover structures that can be hidden from traditional techniques. Combined with a meaningful spatial interpretation which we develop in this paper, these new partial techniques neatly complement the existing techniques, with the potential to help understand and identify dependence structures in complicated multivariate point patterns.

## 9 Competing interests

No competing interest is declared.

## 10 Data availability

The code to reproduce all the simulations and data analysis in this paper is available in the Zenodo repository Grainger (2025a). Code implementing the methodology is available in the `SpatialMultitaper.jl` Julia package (Grainger, 2025b). The Lansing Woods data is available in the `spatstat` R package (Baddeley et al., 2015).

## 11 Acknowledgments

Sofia Olhede would like to thank the European Research Council under Grant CoG 2015-682172NETS, within the Seventh European Union Framework Program.

---

# SUPPLEMENTARY MATERIAL FOR THE PARTIAL $K$ FUNCTION

---

## S1 Table of notation

$d$	Dimension of space.
$P$	Number of point types.
$X, Y, Z$	Point types.
$N$	Ground process containing all point types.
$N_X$	Point process of type $X$ .
$N_X^0$	Centred count measure, $N_X(A) - \lambda_X \ell(A)$ .
$\lambda_X$	Intensity of point process $N_X$ .
$r$	Distance parameter.
$u$	Spatial lag variable.
$s$	Spatial location variable.
$k$	Frequency variable.
$A, B$	Generic measurable sets.
$\ell(B)$	Lebesgue measure of a Borel set $B$ .
$\mathbb{R}^d$	$d$ -dimensional real space.
$\mathbb{N}_0$	Non-negative integers.
$\mathcal{B}(\mathbb{R}^d)$	Borel sets on $\mathbb{R}^d$ .
$\mathbb{U}^2$	Unit square $[0, 1]^2$ .
$S^2$	Unit ball in $\mathbb{R}^2$ .
$S_0^2$	Unit ball minus the origin, $S^2 \setminus \{0\}$ .
$\mathcal{S}_{\mathbb{R}^2}$	Set of totally finite signed measures on $\mathbb{R}^2$ .
$M_{XY}$	Second-order reduced moment measure between point processes $N_X$ and $N_Y$ .
$\check{C}_{XY}$	Second-order reduced cumulant measure between point processes $N_X$ and $N_Y$ .
$K_{XY}$	Ripley's $K$ function between point processes $N_X$ and $N_Y$ .
$L_{XY}$	$L$ function between point processes $N_X$ and $N_Y$ .
$g_{XY}$	Pair correlation function between point processes $N_X$ and $N_Y$ .
$C_{XY}$	$C$ function between point processes $N_X$ and $N_Y$ .
$f_{XY}$	Spectral density function between point processes $N_X$ and $N_Y$ .
$\mathbb{E}[\cdot]$	Expectation operator.
$\text{var}(\cdot)$	Variance operator.
$\ \cdot\ $	The $L^2$ norm.
$x \cdot y$	Dot product between $x$ and $y$ .
$\text{argmin}$	Argument of minimum.
$J_0(\cdot)$	Bessel function of the first kind of order 0.
$J_1(\cdot)$	Bessel function of the first kind of order 1.
$K_{XY \bullet Z}$	Partial $K$ function between point processes $N_X$ and $N_Y$ accounting for point processes $N_Z$ .
$\Lambda_{X \bullet Z}^0$	Centred prediction process.
$\Lambda_{X \bullet Z}$	Prediction process for points of type $X$ predicted linearly from point processes $N_Z$ .
$\lambda_{X \bullet Z}$	Density of $\Lambda_{X \bullet Z}$ .
$\epsilon_{X \bullet Z}$	Residual process for points of type $X$ after linear prediction from point processes $N_Z$ .
$W_{X \bullet Z}$	Prediction kernel for points of type $X$ predicted linearly from point processes $N_Z$ .
$w_{X \bullet Z}$	Density of $W_{X \bullet Z}$ .
$\tilde{w}_{X \bullet Z}$	Fourier transform of $W_{X \bullet Z}$ .
$\hat{w}_{X \bullet Z}$	Estimate of $w_{X \bullet Z}$ .
$h_m$	The $m$ th taper function.
$J_{X;m}$	Tapered Fourier transform of point processes $N_X$ using taper $h_m$ .
$I_{XY;m}$	Single taper periodogram between point processes $N_X$ and $N_Y$ using taper $h_m$ .
$\hat{f}_{XY}$	Multitaper periodogram between point processes $N_X$ and $N_Y$ .
$M$	the number of tapers.

$k_j^\Delta$	the number of wavenumbers used in the $j$ th direction.
$k_j^{\max}$	the maximum wavenumber used in the $j$ th direction.
$L_j$	the length of the bounding box of the observation window in the $j$ th direction.

## S2 Theory

### S2.1 Estimators and summary statistics in the $d$ -dimensional case

In the following subsections, we state the equivalent results in the  $d$ -dimensional case to those given in the main paper.

#### S2.1.1 Summary statistics

Let  $S^d$  be the unit sphere in  $\mathbb{R}^d$  and  $S_0^d = S^d \setminus \{0\}$ . Write  $A_{d-1}$  for the surface area of the unit sphere in  $\mathbb{R}^d$ , then the volume and surface area are

$$\ell(S^d) = \frac{\pi^{d/2}}{\Gamma(d/2 + 1)}, \quad A_{d-1} = \frac{2\pi^{d/2}}{\Gamma(d/2)},$$

respectively.

Best linear prediction is defined simply by replacing  $\mathbb{R}^2$  and  $\mathbb{U}^2$  with  $\mathbb{R}^d$  and  $\mathbb{U}^d$ , respectively, so that

$$\Lambda_{X \bullet Z}^0(A) = \int_{\mathbb{R}^d} W_{X \bullet Z}(A - x) N_Z^0(dx), \quad A \in \mathcal{B}(\mathbb{R}^d),$$

where

$$W_{X \bullet Z} = \underset{W \in \mathcal{S}_{\mathbb{R}^d}}{\operatorname{argmin}} \operatorname{var} \left( N_X^0(\mathbb{U}^d) - \int_{\mathbb{R}^d} W(\mathbb{U}^d - x) N_Z^0(dx) \right).$$

The summary statistics are as follows:

$$\begin{aligned} \lambda_X &= \mathbb{E}[N_X(\mathbb{U}^d)] \\ \check{M}_{XY}(B) &= \mathbb{E} \left[ \int_{\mathbb{U}^d} N_X(B + x) N_Y(dx) \right], \\ \check{C}_{XY}(B) &= \check{M}_{XY}(B) - \lambda_X \lambda_Y \ell(B) \\ K_{XY}(r) &= \lambda_X^{-1} \lambda_Y^{-1} \check{M}_{XY}(r S_0^d) \\ L_{XY}(r) &= \operatorname{sgn}(K_{XY}(r)) \left( \frac{|K_{XY}(r)|}{\ell(S^d)} \right)^{1/d} \\ g_{XY}(r) &= \frac{K'_{XY}(r)}{A_{d-1} r^{d-1}} \\ C_{XY}(r) &= \check{C}_{XY}(r S_0^d) \\ f_{XY}(k) &= \int_{\mathbb{R}^d} e^{-2\pi i u \cdot k} \check{C}_{XY}(du) \end{aligned}$$

Some useful relations used in the main paper in the  $d$ -dimensional case are:

$$\begin{aligned} K_{XY}(r) &= \frac{C_{XY}(r)}{\lambda_X \lambda_Y} + \ell(r S_0^d) \\ g_{XY}(r) &= \frac{C'_{XY}(r)}{A_{d-1} r^{d-1} \lambda_X \lambda_Y} + 1 \\ C_{XY}(r) &= \int_{\mathbb{R}^d} \left( \frac{r}{\|k\|} \right)^{d/2} J_{d/2}(2\pi \|k\| r) [f_{XY}(k) - \check{M}_{XY}(\{0\})] dk \\ C'_{XY}(r) &= 2\pi \int_{\mathbb{R}^d} \|k\| \left( \frac{r}{\|k\|} \right)^{d/2} J_{d/2-1}(2\pi \|k\| r) [f_{XY}(k) - \check{M}_{XY}(\{0\})] dk \end{aligned}$$

### S2.1.2 Estimators

For the second estimator we construct, with an additional rotational averaging, we have in the general case

$$\begin{aligned}\hat{C}_{XY}(r) &= \sum_{\kappa \in K} \hat{f}_{XY}^{(rot)}(\kappa) \int_{\mathbb{R}^d} \mathbb{1}_{(\kappa-\frac{s}{2}, \kappa+\frac{s}{2}]}(\|k\|) \left( \frac{r}{\|k\|} \right)^{d/2} J_{d/2}(2\pi\|k\|r) dk \\ &= \sum_{\kappa \in K} \hat{f}_{XY}^{(rot)}(\kappa) A_{d-1} r^{d/2} \int_{\kappa-s/2}^{\kappa+s/2} x^{d/2-1} J_{d/2}(2\pi x r) dx \\ &= \sum_{\kappa \in K} \hat{f}_{XY}^{(rot)}(\kappa) [w_d(r, \kappa + s/2) - w_d(r, \kappa - s/2)]\end{aligned}$$

where

$$\begin{aligned}w_d(r, y) &= A_{d-1} r^{d/2} \int_0^y x^{d/2-1} J_{d/2}(2\pi x r) dx \\ &= \frac{2(\pi r y)^d}{\Gamma(d/2 + 1)^2} {}_1F_2(d/2; d/2 + 1, d/2 + 1; -(\pi r y)^2).\end{aligned}$$

When  $d = 3$  because  $J_{3/2}(x) = \sqrt{2/\pi x}(\sin(x)/x - \cos(x))$  (see Abramowitz and Stegun (1948) 10.1.11, for example),

$$\begin{aligned}w_3(r, x) &= 4\pi r^{3/2} \int_0^y x^{1/2} J_{3/2}(2\pi x r) dx \\ &= 4\pi r^{3/2} \int_0^y x^{1/2} \sqrt{\frac{2}{2\pi^2 r x}} \left( \frac{\sin(2\pi x r)}{2\pi x r} - \cos(2\pi x r) \right) dx \\ &= 4r \int_0^y \frac{\sin(2\pi x r)}{2\pi x r} - \cos(2\pi x r) dx \\ &= \frac{2}{\pi} \int_0^{2\pi r y} \frac{\sin(z)}{z} - \cos(z) dz \\ &= \frac{2}{\pi} (\text{Si}(2\pi r y) - \sin(2\pi r y))\end{aligned}$$

where

$$\text{Si}(x) = \int_0^x \frac{\sin(y)}{y} dy.$$

For completeness, when  $d = 1$ ,

$$w_1(r, x) = 2\text{Si}(2\pi x r)/\pi.$$

### S2.2 Partial spectra and linear prediction

In the case where we have processes of type  $X, Y$  and a vector of types  $Z = (Z_1, \dots, Z_p)^\top$ , the linear prediction take the form

$$\Lambda_{X \bullet Z}^0(A) = \sum_{j=1}^p \int_{\mathbb{R}^2} W_j(A - z) N_{Z_j}^0(dz),$$

analogously to the time series case (Brillinger, 1974).

**Proposition S1.** *Say we have homogeneous point processes processes of type  $X, Y$  and a vector of types  $Z = (Z_1, \dots, Z_p)^\top$ . Assume that all reduced covariance measures are totally finite and writing  $U = (X, Y, Z^\top)^\top$ , that the spectral matrix  $f_{UU}(k)$  is invertible for all  $k \in \mathbb{R}^d$ . Then, the Fourier transform of the kernel in the best linear prediction of  $X$  from  $Z$  is given by*

$$\tilde{w}_{X \bullet Z}(k) = f_{XZ}(k) f_{ZZ}(k)^{-1}.$$

*Proof.* We have

$$\begin{aligned} \text{var} \left( N_X^0(\mathbb{U}^d) - \int_{\mathbb{R}^d} W(\mathbb{U}^d - x) N_Z^0(dx) \right) &= \text{var} (N_X^0(\mathbb{U}^d)) + \text{var} \left( \int_{\mathbb{R}^d} W(\mathbb{U}^d - x) N_Z^0(dx) \right) \\ &\quad - 2 \operatorname{Re} \operatorname{cov} \left( N_X^0(\mathbb{U}^d), \int_{\mathbb{R}^d} W(\mathbb{U}^d - x) N_Z^0(dx) \right) \end{aligned}$$

Proceeding with each term in turn, firstly

$$\begin{aligned} \text{var} (N_X^0(\mathbb{U}^d)) &= \int_{\mathbb{R}^{2d}} \mathbb{1}_{\mathbb{U}^d}(x) \mathbb{1}_{\mathbb{U}^d}(y) C_{XX}(dx \times dy) \\ &= \int_{\mathbb{R}^d} \int_{\mathbb{R}^d} \mathbb{1}_{\mathbb{U}^d}(z+u) \mathbb{1}_{\mathbb{U}^d}(z) \ell(dz) \check{C}_{XX}(du) \\ &= \int_{\mathbb{R}^d} |\tilde{\mathbb{1}}_{\mathbb{U}^d}(k)|^2 f_{XX}(k) dk. \end{aligned}$$

Secondly

$$\text{var} \left( \int_{\mathbb{R}^d} W(\mathbb{U}^d - x) N_Z^0(dx) \right) = \int_{\mathbb{R}^d} |\tilde{\mathbb{1}}_{\mathbb{U}^d}(k)|^2 |\tilde{w}(k)|^2 f_{ZZ}(k) dk.$$

where  $\tilde{w}(k) = \int_{\mathbb{R}^d} e^{-2\pi i x \cdot k} W(dx)$  is the Fourier transform of  $W$ . Finally, we have

$$\operatorname{cov} \left( N_X^0(\mathbb{U}^d), \int_{\mathbb{R}^d} W(\mathbb{U}^d - x) N_Z^0(dx) \right) = \int_{\mathbb{R}^d} |\tilde{\mathbb{1}}_{\mathbb{U}^d}(k)|^2 \tilde{w}(k) f_{XZ}(k) dk.$$

Therefore we see

$$\begin{aligned} \text{var} \left( N_X^0(\mathbb{U}^d) - \int_{\mathbb{R}^d} W(\mathbb{U}^d - x) N_Z^0(dx) \right) &= \int_{\mathbb{R}^d} |\tilde{\mathbb{1}}_{\mathbb{U}^d}(k)|^2 \left( f_{XX}(k) - 2 \operatorname{Re} \{ \tilde{w}(k) f_{XZ}(k) \} + |\tilde{w}(k)|^2 f_{ZZ}(k) \right) dk. \end{aligned}$$

We then want to choose  $\tilde{w}$  to minimise Section S2.2. This is achieved if we choose  $\tilde{w}$  so that

$$f_{XX}(k) - 2 \operatorname{Re} \{ \tilde{w}(k) f_{XZ}(k) \} + |\tilde{w}(k)|^2 f_{ZZ}(k)$$

is minimised for all  $k \in \mathbb{R}^d$ .

For all  $k \in \mathbb{R}^d$ , the minimizer is

$$\tilde{w}(k) = \frac{f_{XZ}(k)}{f_{ZZ}(k)}.$$

When  $Z$  is multivariate, an analogous argument holds and for all  $k \in \mathbb{R}^d$

$$\tilde{w}(k) = f_{XZ}(k) f_{ZZ}(k)^{-1},$$

where  $\tilde{w}(k)$  is now a vector (as in the time series case (Brillinger, 1974) or random fields (Guinness et al., 2014)).  $\square$

**Proposition S2.** *Under the conditions of Proposition S1, the partial spectra between  $X$  and  $Y$  accounting for  $Z$  is*

$$f_{XY \bullet Z}(k) = f_{XY}(k) - f_{XZ}(k) f_{ZZ}(k)^{-1} f_{ZY}(k),$$

for all  $k \in \mathbb{R}^d$ .

*Proof.* We have, from a similar bilinearity of covariance type argument as the proof of Proposition S1,

$$\begin{aligned} f_{\epsilon_{X \bullet Z}, \epsilon_{Y \bullet Z}}(k) &= f_{XY}(k) - f_{X \Lambda_Y \bullet Z}(k) - f_{\Lambda_X \bullet Z Y}(k) + f_{\Lambda_X \bullet Z \Lambda_Y \bullet Z}(k) \\ &= f_{XY}(k) - f_{XZ}(k) \tilde{w}_{Y \bullet Z}(k)^H - \tilde{w}_{X \bullet Z}(k) f_{ZY}(k) + \tilde{w}_{X \bullet Z}(k) f_{ZZ}(k) \tilde{w}_{Y \bullet Z}^H(k) \\ &= f_{XY}(k) - f_{XZ}(k) (f_{YZ}(k) f_{ZZ}(k)^{-1})^H - (f_{XZ}(k) f_{ZZ}(k)^{-1}) f_{ZY}(k) \\ &\quad + (f_{XZ}(k) f_{ZZ}(k)^{-1}) f_{ZZ}(k) (f_{YZ}(k) f_{ZZ}(k)^{-1})^H \\ &= f_{XY}(k) - f_{XZ}(k) f_{ZZ}(k)^{-1} f_{ZY}(k). \end{aligned}$$

Where the final line follows from conjugate symmetry of the spectral density matrix.  $\square$

**Proposition S3.** *Under the conditions of Proposition S1, the partial spectra between  $X$  and  $Y$  accounting for  $Z$  corresponds to the spectra between  $\Lambda_{X \bullet Z}$  and  $Y$ .*

*Proof.* Directly from the proof of Proposition S2, we see, omitting the  $(k)$  for convenience

$$\begin{aligned} f_{XY \bullet Z} - f_{\epsilon_{X \bullet Z} Y} &= f_{XY} - f_{X \Lambda_{Y \bullet Z}} - f_{\Lambda_{X \bullet Z} Y} + f_{\Lambda_{X \bullet Z} \Lambda_{Y \bullet Z}} - f_{XY} + f_{\Lambda_{X \bullet Z} Y} \\ &= f_{\Lambda_{X \bullet Z} \Lambda_{Y \bullet Z}} - f_{X \Lambda_{Y \bullet Z}} \\ &= f_{XZ} f_{ZZ}^{-1} f_{ZY} - f_{XZ} f_{ZZ}^{-1} f_{ZY} \\ &= 0. \end{aligned}$$

□

### S2.3 The spectral density function and C function

Following Daley and Vere-Jones (2003), write

$$\tilde{e}_\lambda(k) = \prod_{j=1}^d \frac{\lambda^2}{\lambda^2 + k_j^2}.$$

Then we have the inverse relation

$$\check{C}_{XY}(B) = \lim_{\lambda \rightarrow \infty} \int_{\mathbb{R}^d} \tilde{e}_\lambda(k) \tilde{\mathbb{1}}_B(k) f_{XY}(k) dk,$$

for continuity sets of  $\check{C}_{XY}$  (Daley and Vere-Jones, 2003). Define  $D_{XY}(B) = \check{C}_{XY}(B \cap \{0\})$ , then

$$D_{XY}(B) = \lim_{\lambda \rightarrow \infty} \int_{\mathbb{R}^d} \tilde{e}_\lambda(k) \tilde{\mathbb{1}}_B(k) \check{M}_{XY}(\{0\}) dk,$$

for continuity sets of  $D_{XY}$  (which includes continuity sets of  $\check{C}_{XY}$ ). Therefore, we have

$$\begin{aligned} \check{C}_{XY}(B \setminus \{0\}) &= \check{C}_{XY}(B) - D_{XY}(B) \\ &= \lim_{\lambda \rightarrow \infty} \int_{\mathbb{R}^d} \tilde{e}_\lambda(k) \tilde{\mathbb{1}}_B(k) [f_{XY}(k) - \check{M}_{XY}(\{0\})] dk \\ &= \int_{\mathbb{R}^d} \tilde{\mathbb{1}}_B(k) [f_{XY}(k) - \check{M}_{XY}(\{0\})] dk, \end{aligned}$$

provided that  $f_{XY}(k) - \check{M}_{XY}(\{0\})$  is integrable.

As a result, we can recover the reduced cumulant measure from the spectral density function, meaning that we could also recover Ripley's  $K$  function from the spectral density function and the intensities. We have

$$\tilde{\mathbb{1}}_{rS^d}(k) = \begin{cases} \ell(rS^d) & \text{if } k = 0, \\ (r/\|k\|)^{d/2} J_{d/2}(2\pi\|k\|r) & \text{otherwise.} \end{cases}$$

Furthermore

$$\frac{\partial}{\partial r} \tilde{\mathbb{1}}_{rS^d}(k) = \begin{cases} A_{d-1} r^{d-1} & \text{if } k = 0, \\ 2\pi\|k\|(r/\|k\|)^{d/2} J_{d/2-1}(2\pi\|k\|r) & \text{otherwise.} \end{cases}$$

Therefore because  $[f_{XY}(k) - \check{M}_{XY}(\{0\})]$  is integrable, we can interchange limits by Leibniz integral rule and

$$\begin{aligned} C_{XY}(r) &= \int_{\mathbb{R}^d} \left( \frac{r}{\|k\|} \right)^{d/2} J_{d/2}(2\pi\|k\|r) [f_{XY}(k) - \check{M}_{XY}(\{0\})] dk, \\ C'_{XY}(r) &= 2\pi r \int_{\mathbb{R}^d} \left( \frac{r}{\|k\|} \right)^{d/2-1} J_{d/2-1}(2\pi\|k\|r) [f_{XY}(k) - \check{M}_{XY}(\{0\})] dk. \end{aligned}$$

In particular, when  $d = 2$

$$\begin{aligned} C_{XY}(r) &= \int_{\mathbb{R}^2} \frac{r}{\|k\|} J_1(2\pi\|k\|r) [f_{XY}(k) - \check{M}_{XY}(\{0\})] dk, \\ C'_{XY}(r) &= 2\pi r \int_{\mathbb{R}^2} J_0(2\pi\|k\|r) [f_{XY}(k) - \check{M}_{XY}(\{0\})] dk. \end{aligned}$$

## S2.4 Bias correction

Say that we have  $P$  point processes. In addition, we use a multitaper spectral estimate with a fixed  $M > P$  tapers. We will be interested in a growing domain framework, as in Grainger et al. (2025). In order to do this, we will write  $\hat{f}_n(k)$  for the spectral density matrix function estimate at wavenumber  $k$  from the  $n$ th observational window in a sequence of growing windows.

We need some preliminary results before obtaining our required bias results. This first Lemma is Theorem 3.6 of Andersen et al. (1995).

**Lemma S1.** *Consider a complex Wishart distributed random variable  $X \sim \mathcal{W}_m^C(n, \Sigma)$ . Say that  $X$  is partitioned so that*

$$X = \begin{bmatrix} X_{11} & X_{12} \\ X_{21} & X_{22} \end{bmatrix}$$

*with  $X_{11}$  being  $s \times s$  (so  $X_{22}$  is  $m - s \times m - s$ ). Then if  $X_{11 \bullet 2} = X_{11} - X_{12}X_{22}^{-1}X_{21}$  we have*

$$X_{11 \bullet 2} \sim \mathcal{W}_s^C(n - (m - s), \Sigma_{11 \bullet 2}).$$

**Lemma S2.** *Under assumptions 1-5 and 7 of Grainger et al. (2025), we have that for a fixed number of processes  $P$  and a fixed number of tapers  $M$*

$$\hat{f}_n(k) \xrightarrow{d} \mathcal{W}_P^C(M, f(k)/M)$$

*Proof.* This follows from Theorem 3 of Grainger et al. (2025) and the continuous mapping theorem.  $\square$

Now in order to use this result for the expectation, we need to establish uniform integrability conditions. Strictly speaking, we do not have guarantees that the multitaper periodogram is invertible almost surely. Therefore, since it is a Gram matrix, and thus positive-semi definite, we can consider instead the generalised schur complement (Carlson et al., 1974), defined by

$$\hat{f}_{11 \bullet 2; n}^\dagger = \hat{f}_{11; n} - \hat{f}_{12; n} \hat{f}_{22; n}^+ \hat{f}_{21; n}$$

where  $\hat{f}_{22; n}^+$  is the Moore-Penrose pseudoinverse of  $\hat{f}_{22; n}$ . This is well-defined almost surely.

**Lemma S3.** *Writing  $\|\cdot\|_F$ , say that there exists  $\delta > 0$  such that  $\sup_{n \in \mathbb{N}} \mathbb{E} \left[ \left\| \hat{f}_n \right\|_F^{1+\delta} \right] < \infty$ . Then we have*

$$\sup_{n \in \mathbb{N}} \mathbb{E} \left[ \left\| \hat{f}_{11 \bullet 2; n}^\dagger \right\|_F^{1+\delta} \right] < \infty.$$

*Proof.* We have

$$\begin{aligned} \hat{f}_{11; n} - \hat{f}_{11 \bullet 2; n} &= \hat{f}_{12; n} \hat{f}_{22; n}^+ \hat{f}_{21; n} \\ &= \hat{f}_{12; n} \hat{f}_{22; n}^+ \hat{f}_{12; n}^H \\ &\succeq 0, \end{aligned}$$

because  $\hat{f}_{22; n}$  is Hermitian and positive semi-definite and therefore so is  $\hat{f}_{22; n}^+$  by Theorem 29.6 of Ben-Israel and Greville (2003). Therefore, in Loewner order,  $\hat{f}_{11; n} \succeq \hat{f}_{11 \bullet 2; n}$ . As a result, writing  $\|\cdot\|_F$  for the Frobenius norm (which is monotone on the space of positive semi-definite matrices (Ciarlet et al., 1989)), we have

$$\left\| \hat{f}_{11 \bullet 2; n}^\dagger \right\|_F \leq \left\| \hat{f}_{11; n} \right\|_F \leq \left\| \hat{f}_n \right\|_F$$

almost surely, and therefore

$$\sup_{n \in \mathbb{N}} \mathbb{E} \left[ \left\| \hat{f}_{n, 11 \bullet 2} \right\|_F^{1+\delta} \right] \leq \sup_{n \in \mathbb{N}} \mathbb{E} \left[ \left\| \hat{f}_n \right\|_F^{1+\delta} \right] < \infty,$$

as required.  $\square$

**Lemma S4.** *Assuming fourth-order moment conditions already required for Lemma S2, we have*

$$\sup_{n \in \mathbb{N}} \mathbb{E} \left[ \left\| \hat{f}_n \right\|_F^2 \right] < \infty.$$

*Proof.* This follows from the convergence of the mean and variance of the multitaper periodogram to finite values established in Grainger et al. (2025) in the proof of Theorem 3.  $\square$

**Theorem S1.** *Given the conditions of the other results in this section, we have*

$$\mathbb{E} \left[ \hat{f}_{11 \bullet 2; n}(k) \right] \rightarrow \frac{M + s - P}{M} f_{11 \bullet 2}(k)$$

as  $n \rightarrow \infty$ . Note that  $P - s = P_Z$  in the notation of the main paper.

*Proof.* As established,  $\hat{f}_n \xrightarrow{d} \mathcal{W}_P^C(M, f(k)/M)$ . Now we again need to use the continuous mapping theorem for the generalised Schur complement. Though the generalised Schur complement is not continuous everywhere, it is continuous almost surely with respect to the Wishart distribution with positive definite covariance (which we have by assumption). Therefore we have  $\hat{f}_{11 \bullet 2; n} \xrightarrow{d} \mathcal{W}_s^C(M - (P - s), \Sigma_{11 \bullet 2}/M)$ . Furthermore, we also have uniform integrability, and so from standard results (Billingsley, 2012, Theorem 25.12)

$$\mathbb{E} \left[ \hat{f}_{11 \bullet 2; n}(k) \right] \rightarrow \mathbb{E} [A]$$

where  $A \sim \mathcal{W}_s^C(M - (P - s), f_{11 \bullet 2}(k)/M)$ . Finally, by properties of the complex Wishart distribution

$$\mathbb{E} [A] = (M + s - P) f_{11 \bullet 2}(k)/M$$

yielding the desired result.  $\square$

## S2.5 Fast computation

The formulae for obtaining partial spectra given above are not the most efficient way to construct them (Dahlhaus, 2000). The alternate formulae, from Dahlhaus (2000) and Eichler et al. (2003) continue to hold in this setting, as they are just related to matrix manipulations. In particular omitting the  $k$  argument, let  $g = f^{-1}$  be the function which is the inverse of  $f$  at each wavenumber  $k$  (not the inverse function), and write  $g_{XY}$  to mean the  $XY$  element of  $g$ . Then from Eichler et al. (2003) we have

$$\begin{aligned} f_{XX \bullet (YZ)} &= \frac{1}{g_{XX}}, \\ R_{XY \bullet Z} &= \frac{f_{XY \bullet Z}}{\sqrt{f_{XX \bullet Z} f_{YY \bullet Z}}} = \frac{-g_{XY}}{\sqrt{g_{XX} g_{YY}}}, \\ f_{XY \bullet Z} &= \frac{R_{XY}}{1 - |R_{XY}|^2} \sqrt{f_{XX \bullet (YZ)} f_{YY \bullet (XZ)}}. \end{aligned}$$

Note there is a difference between  $f_{XX \bullet (YZ)}$  and  $f_{XX \bullet Z}$ . We are interested in  $f_{XX \bullet (YZ)}$  and  $f_{XY \bullet Z}$ . Writing these entirely in terms of  $g$ , we have

$$\begin{aligned} f_{XY \bullet Z} &= \frac{R_{XY}}{1 - |R_{XY}|^2} \sqrt{f_{XX \bullet (YZ)} f_{YY \bullet (XZ)}} \\ &= \frac{-g_{XY}/\sqrt{g_{XX} g_{YY}}}{1 - |g_{XY}|^2/g_{XX} g_{YY}} \frac{1}{\sqrt{g_{XX} g_{YY}}} \\ &= \frac{-g_{XY}}{g_{XX} g_{YY} - |g_{XY}|^2}. \end{aligned}$$

So in summary

$$\begin{aligned} f_{XX \bullet (YZ)} &= \frac{1}{g_{XX}}, \\ f_{XY \bullet Z} &= \frac{-g_{XY}}{g_{XX} g_{YY} - |g_{XY}|^2}. \end{aligned}$$

## S2.6 Counterexample to conditional orthogonality

Consider the following setup. Let  $N_Z$  be a homogeneous Poisson process with intensity  $\lambda_Z > 0$  on  $\mathbb{R}^d$ . Now let  $\Lambda(u) = [\int_{\mathbb{R}^d} g(u-x)N_Z(dx)]^2$  for some kernel  $g : \mathbb{R}^d \rightarrow [0, \infty)$ . Then let  $N_X$  be a Cox process driven by  $\Lambda$  and  $N_Y$  also be a Cox process driven by  $\Lambda$  but independent of  $N_X$  given  $\Lambda$ . For notational convenience, write  $\lambda = \lambda_Z$ . Then we have

$$\begin{aligned}
\mathbb{E}[\Lambda(u)\Lambda(0)] &= \mathbb{E}\left[\left[\int_{\mathbb{R}^d} g(u-w)N_Z(dw)\right]^2 \left[\int_{\mathbb{R}^d} g(-y)N_Z(dy)\right]^2\right] \\
&= \mathbb{E}\left[\int_{\mathbb{R}^d} \int_{\mathbb{R}^d} \int_{\mathbb{R}^d} \int_{\mathbb{R}^d} g(u-w)g(u-x)g(-y)g(-z)N_Z(dw)N_Z(dx)N_Z(dy)N_Z(dz)\right] \\
&= \int_{\mathbb{R}^d} \int_{\mathbb{R}^d} \int_{\mathbb{R}^d} \int_{\mathbb{R}^d} g(u-w)g(u-x)g(-y)g(-z)M_{ZZZZ}(dw \times dx \times dy \times dz) \\
&= \lambda^4 \int_{\mathbb{R}^d} \int_{\mathbb{R}^d} \int_{\mathbb{R}^d} \int_{\mathbb{R}^d} g(u-w)g(u-x)g(-y)g(-z)dw dx dy dz \\
&\quad + \lambda^3 \int_{\mathbb{R}^d} \int_{\mathbb{R}^d} \int_{\mathbb{R}^d} g(u-w)^2 g(-y)g(-z)dw dy dz \\
&\quad + 4\lambda^3 \int_{\mathbb{R}^d} \int_{\mathbb{R}^d} \int_{\mathbb{R}^d} g(u-w)g(u-x)g(-w)g(-z)dw dx dz \\
&\quad + \lambda^3 \int_{\mathbb{R}^d} \int_{\mathbb{R}^d} \int_{\mathbb{R}^d} g(u-w)g(u-x)g(-y)^2 dw dx dy \\
&\quad + \lambda^2 \int_{\mathbb{R}^d} \int_{\mathbb{R}^d} g(u-w)^2 g(-y)^2 dw dy \\
&\quad + 2\lambda^2 \int_{\mathbb{R}^d} \int_{\mathbb{R}^d} g(u-w)g(u-x)g(-x)g(-w)dw dx \\
&\quad + 2\lambda^2 \int_{\mathbb{R}^d} \int_{\mathbb{R}^d} g(u-w)^2 g(-w)g(-z)dw dz \\
&\quad + 2\lambda^2 \int_{\mathbb{R}^d} \int_{\mathbb{R}^d} g(u-w)g(u-x)g(-w)^2 dw dx \\
&\quad + \lambda \int_{\mathbb{R}^d} \int_{\mathbb{R}^d} g(u-w)g(u-w)g(-w)g(-w)dw \\
&= \lambda^4 \|g\|_1^4 + 2\lambda^3 \|g\|_2^2 \|g\|_1^2 + 4\lambda^3 \|g\|_1^2 [g * g^*](u) + \lambda^2 \|g\|_2^4 + 2\lambda^2 [g * g^*](u)^2 \\
&\quad + 2\lambda^2 \|g\|_1 [g^2 * g^*](u) + 2\lambda^2 \|g\|_1 [g^2 * g^*](-u) + \lambda [g^2 * (g^*)^2](u)
\end{aligned}$$

Additionally, we have

$$\begin{aligned}
\mathbb{E}[\Lambda(u)] &= \mathbb{E}\left[\left[\int_{\mathbb{R}^d} g(u-x)N_Z(dx)\right]^2\right] \\
&= \lambda^2 \|g\|_1^2 + \lambda \|g\|_2^2.
\end{aligned}$$

Therefore

$$\begin{aligned}
\check{c}_{\Lambda\Lambda}(u) &= \lambda^4 \|g\|_1^4 + 2\lambda^3 \|g\|_2^2 \|g\|_1^2 + 4\lambda^3 \|g\|_1^2 [g * g^*](u) + \lambda^2 \|g\|_2^4 + 2\lambda^2 [g * g^*](u)^2 \\
&\quad + 2\lambda^2 \|g\|_1 [g^2 * g^*](u) + 2\lambda^2 \|g\|_1 [g^2 * g^*](-u) + \lambda [g^2 * (g^*)^2](u) \\
&\quad - \left(\lambda^2 \|g\|_1^2 + \lambda \|g\|_2^2\right)^2 \\
&= 4\lambda^3 \|g\|_1^2 [g * g^*](u) + 2\lambda^2 \{[g * g^*](u)^2 + \|g\|_1 [g^2 * g^*](u) + \|g\|_1 [g^2 * g^*](-u)\} \\
&\quad + \lambda [g^2 * (g^*)^2](u).
\end{aligned}$$

As a result, we have

$$f_{\Lambda\Lambda}(k) = 4\lambda^3 \|g\|_1^2 |G(k)|^2 + 2\lambda^2 \left\{ [|G|^2 * |G|^2](k) + 2\|g\|_1 \operatorname{Re}([G * G](k) \overline{G(k)}) \right\} + \lambda |[G * G](k)|^2$$

Now we have

$$\begin{aligned} f_{XX}(k) &= f_{YY}(k) = f_{\Lambda\Lambda}(k) + \lambda_{\Lambda} \\ f_{XY}(k) &= f_{\Lambda\Lambda}(k). \end{aligned}$$

Finally,

$$\begin{aligned} \check{M}_{Z\Lambda}(B) &= \mathbb{E} \left[ \int_{\mathbb{U}^d} \Lambda(B+z) N_Z(dz) \right] \\ &= \mathbb{E} \left[ \int_{\mathbb{U}^d} \int_B \left[ \int_{\mathbb{R}^d} g(u-x) N_Z(dx) \right]^2 du N_Z(dz) \right] \\ &= \int_B \int_{\mathbb{R}^d} \int_{\mathbb{R}^d} \int_{\mathbb{R}^d} \mathbb{1}_{\mathbb{U}^d}(z) g(u+z-x) g(u+z-y) M_{ZZZ}(dx \times dy \times dz) \\ &= \int_B \lambda^3 \|g\|_1^2 + \lambda^2 \|g\|_2^2 + 2\lambda^2 \int_{\mathbb{R}^d} \int_{\mathbb{R}^d} \mathbb{1}_{\mathbb{U}^d}(z) g(u) g(u+z-y) dy dz \\ &\quad + \lambda \int g(u)^2 \mathbb{1}_{\mathbb{U}^d}(z) dz du \\ &= \int_B \lambda^3 \|g\|_1^2 + \lambda^2 \|g\|_2^2 + 2\lambda^2 \|g\|_1 g(u) + \lambda g(u)^2 du \end{aligned}$$

Therefore, see  $\check{M}_{Z\Lambda}(B)$  has density

$$\check{m}_{Z\Lambda}(u) = \lambda^3 \|g\|_1^2 + \lambda^2 \|g\|_2^2 + 2\lambda^2 \|g\|_1 g(u) + \lambda g(u)^2.$$

So

$$\begin{aligned} \check{c}_{Z\Lambda}(u) &= \lambda^3 \|g\|_1^2 + \lambda^2 \|g\|_2^2 + 2\lambda^2 \|g\|_1 g(u) + \lambda g(u)^2 - \lambda(\lambda^2 \|g\|_1^2 + \lambda \|g\|_2^2) \\ &= 2\lambda^2 \|g\|_1 g(u) + \lambda g(u)^2 \end{aligned}$$

Therefore

$$f_{Z\Lambda}(k) = 2\lambda^2 \|g\|_1 G(k) + \lambda [G * G](k).$$

Furthermore,  $f_{ZX} = f_{ZY} = f_{Z\Lambda}$ .

Now we can compute the partial spectra

$$\begin{aligned} f_{XY \bullet Z} &= f_{XY} - f_{XZ} f_{ZZ}^{-1} f_{ZY} \\ &= f_{XY} - \lambda^{-1} \overline{f_{ZX}} f_{ZY} \\ &= f_{XY} - \lambda^{-1} |f_{Z\Lambda}| \end{aligned}$$

so for all  $k \in \mathbb{R}^d$

$$\begin{aligned} f_{XY \bullet Z}(k) &= f_{XY} - |2\lambda^2 \|g\|_1 G(k) + \lambda [G * G](k)|^2 / \lambda \\ &= f_{XY} - 4\lambda^3 \|g\|_1^2 |G(k)|^2 + 2\lambda^2 \operatorname{Re}([G * G](k) \overline{G(k)}) + \lambda |[G * G](k)|^2 \\ &= 2\lambda^2 [|G|^2 * |G|^2](k) \end{aligned}$$

This is not equal to zero everywhere (unless  $g = 0$  almost everywhere, which corresponds to having no points of type  $X$  or  $Y$  almost surely).

### S3 Resampling

One common approach to inference for point processes is to compute null envelopes for the statistic of interest, see (Myllymäki et al., 2017) for example. This typically requires simulation under the null of choice. In the univariate case, the null is usually that the process is a Poisson process, and so we simply simulate from a Poisson process with an intensity equal to the estimated intensity from the observed point pattern. In the bivariate case, Mrkvička et al. (2021) review some common methods for performing null resampling, when the null hypothesis is that the two processes are independent. The essence of the resampling is to shift one of the two patterns randomly relative to the other, breaking

their cross dependence, but retaining marginal properties. Various schemes are designed to deal with boundary problems which arise from this shifting (Mrkvička et al., 2021).

The null in our case is more complicated as it is not a pair of processes which we claim are uncorrelated, but rather the residual processes. Ideally, if we have realisations of the residuals, we could shift those using a similar strategy to those described by Mrkvička et al. (2021). However, we do not have direct access to these residuals. Such resampling in our case is tricky, and remains an open problem, however, we will briefly discuss some of the approaches which we have considered.

Firstly let us consider the intraprocess case. In this case, in fact, the solution is theoretically straightforward, but practically difficult. An analogous null to the standard case if we are interested in the partial  $K$  function between  $X$  and itself accounting for  $Z$ , is to simulate from an inhomogeneous Poisson process with intensity given by  $\Lambda_{X \bullet Z}$ . In practice then, we could replace  $\Lambda_{X \bullet Z}$  with some form of estimate. However, this approach is sensitive in practice.

In the interprocess case, the problem is even more difficult. Say that we are interested in the partial  $K$  function between  $X$  and  $Y$  accounting for  $Z$ . Then the null hypothesis is that the residual process of  $X$  with  $Z$  and the residual process of  $Y$  with  $Z$  are uncorrelated. There are three approaches we could immediately consider here. The first is to apply the standard shifting approaches (Mrkvička et al., 2021) to all of the processes involved, and then compute the partial  $K$  function between the shifted processes. This has the advantage of being simple to implement, but has the disadvantage that we make all of the different processes independent, rather than just the residuals. The second approach would be to shift only the  $X$  process say, breaking the dependence between the residual processes, but also breaking some of the other dependences. The third approach would be to again simulate from inhomogeneous Poisson processes with intensities given by  $\Lambda_{X \bullet Z}$  and  $\Lambda_{Y \bullet Z}$  respectively.

Say that we are in the cross-process case, and we have processes of interest  $X$  and  $Y$ , and covariate processes  $Z$ . Then there are essentially (due to symmetries) 6 quantities of interest:  $f_{XX}$ ,  $f_{YY}$ ,  $f_{ZZ}$ ,  $f_{XY}$ ,  $f_{XZ}$ ,  $f_{YZ}$ . Now, the partial spectra of interest is  $f_{XY \bullet Z} = f_{XY} - f_{XZ}f_{ZZ}^{-1}f_{ZY}$ . We want the resampling method to set  $f_{XY \bullet Z}$  to zero, whilst maintaining  $f_{XX}$ ,  $f_{YY}$ ,  $f_{XZ}$ ,  $f_{YZ}$  and  $f_{ZZ}$ . In other words, by setting  $f_{XY} = f_{XZ}f_{ZZ}^{-1}f_{ZY}$ . However, none of the methods we have previously discussed achieve this exactly. Table 1 summarises the effects of the different resampling methods on the different components of the spectral density function. In pilot simulation studies, we have found that these approaches can perform well in some scenarios, but when there is strong dependence between the processes, they can fail to achieve the desired Type I error rate, in some cases catastrophically (we saw rejection rates around 40% when the nominal level was 5%). Therefore, this aspect requires further research.

Component	Ideal Method	Shift all	Shift $X$	Cox Generation
$f_{XX}$	—	—	—	$f_{XZ}f_{ZZ}^{-1}f_{ZX} + \lambda_X$
$f_{YY}$	—	—	—	$f_{YZ}f_{ZZ}^{-1}f_{ZY} + \lambda_Y$
$f_{ZZ}$	—	—	—	—
$f_{XY}$	$f_{XZ}f_{ZZ}^{-1}f_{ZY}$	0	0	$f_{XZ}f_{ZZ}^{-1}f_{ZY}$
$f_{XZ}$	—	0	0	—
$f_{YZ}$	—	0	—	—

Table 1: Effects of different resampling methods on spectral density components. A — indicates that a component is preserved.

## S4 Example models

### S4.1 Model definition

Consider the following simple model. Say that  $Z$  is a homogeneous Poisson process with intensity  $\lambda_Z$ . Say that  $X$  and  $Y$  are generated by cluster processes, which cluster independently around  $Z$  points, with  $\text{Poisson}(\eta_X)$  points per  $X$  cluster and  $\text{Poisson}(\eta_Y)$  points per  $Y$  cluster. Say that the distribution of the difference of the point from its parent are given by  $\text{Poisson}(\eta_X)$  and  $\text{Poisson}(\eta_Y)$  for points of type  $X$  and  $Y$  respectively. If they have densities, we will write  $p_X$  and  $p_Y$ .

## S4.2 Model properties

Then one can rewrite the cluster process as a Cox process with the driving intensity measure

$$\Lambda_X(B) = \eta_X \int_{\mathbb{R}^d} P_X(B-u) N_Z(\mathrm{d}u),$$

and similarly for  $N_Y$  (Daley and Vere-Jones, 2003).

**Lemma S5.** *We have the following reduced moment measures*

$$\begin{aligned}\check{M}_{XZ}(B) &= \eta_X \int_{\mathbb{R}^d} P_X(B-u) \check{M}_{ZZ}(\mathrm{d}u), \\ \check{M}_{XY}(B) &= \eta_X \eta_Y \int_{\mathbb{R}^d} \int_{\mathbb{R}^d} P_X(B+y'-u) P_Y(\mathrm{d}y') \check{M}_{ZZ}(\mathrm{d}u), \\ \check{M}_{XX}(B) &= \eta_X \lambda_Z \delta(B) + \eta_X^2 \int_{\mathbb{R}^d} \int_{\mathbb{R}^d} P_X(B+y'-u) P_X(\mathrm{d}y') \check{M}_{ZZ}(\mathrm{d}u),\end{aligned}$$

where  $\delta$  is the Dirac measure.

**Lemma S6.** *If  $P_X$  and  $P_Y$  admit densities  $p_X$  and  $p_Y$ , then the reduced moment measures admit densities (except for the atom at zero), so that*

$$\begin{aligned}\check{m}_{XZ}(x) &= \eta_X \int_{\mathbb{R}^d} p_X(x-u) \check{M}_{ZZ}(\mathrm{d}u), \\ \check{m}_{XY}(x) &= \eta_X \eta_Y \int_{\mathbb{R}^d} \int_{\mathbb{R}^d} p_X(x+y'-u) p_Y(y') \ell(\mathrm{d}y') \check{M}_{ZZ}(\mathrm{d}u), \\ \check{m}_{XX}(x) &= \eta_X \lambda_Z \delta(x) + \eta_X^2 \int_{\mathbb{R}^d} \int_{\mathbb{R}^d} p_X(x+y'-u) p_X(y') \ell(\mathrm{d}y') \check{M}_{ZZ}(\mathrm{d}u)\end{aligned}$$

where here  $\delta$  means the Dirac delta function.

For the distribution  $P_X$ , we will write

$$\phi_X(k) = \int_{\mathbb{R}^d} e^{2\pi i x \cdot k} P_X(\mathrm{d}x)$$

to be the characteristic function (the inverse Fourier transform of the distribution). Note we are including the factor of  $2\pi$  in our convention.

**Lemma S7.** *We have the following spectral density functions (with the remaining coming from relabelling and symmetry)*

$$\begin{aligned}f_{XZ}(k) &= \eta_X \overline{\phi_X(k)} f_{ZZ}(k), \\ f_{XY}(k) &= \eta_X \eta_Y \overline{\phi_X(k)} \phi_Y(k) f_{ZZ}(k), \\ f_{XX}(k) &= \eta_X \lambda_Z + \eta_X^2 |\phi_X(k)|^2 f_{ZZ}(k).\end{aligned}$$

**Proposition S4.** *The partial spectra for the cluster model are*

$$\begin{aligned}f_{XY \bullet Z}(k) &= 0, \\ f_{X, Z \bullet Y}(k) &= \frac{\eta_X \lambda_Z \overline{\phi_X(k)} f_{ZZ}(k)}{\lambda_Z + \eta_Y |\phi_Y(k)|^2 f_{ZZ}(k)}, \\ f_{X, X \bullet Y, Z}(k) &= \lambda_X, \\ f_{Z, Z \bullet X, Y}(k) &= \frac{\lambda_Z f_{ZZ}(k)}{\eta_Y |\phi_Y(k)|^2 f_{ZZ}(k) + \eta_X |\phi_X(k)|^2 f_{ZZ}(k) + \lambda_Z}.\end{aligned}$$

## S4.3 Proofs of model properties

Let  $M_{XY}$  be the joint moment measure of  $N_X$  and  $N_Y$  so that  $M_{XY}(A \times B) = \mathbb{E}[N_X(A)N_Y(B)]$  for  $A, B \in \mathcal{B}(\mathbb{R}^d)$ . This relates to the reduced moment measure by

$$\int_{\mathbb{R}^{2d}} g(x, y) M_{XY}(\mathrm{d}x \times \mathrm{d}y) = \int_{\mathbb{R}^d} \int_{\mathbb{R}^d} g(z+u, z) \check{M}_{XY}(\mathrm{d}u) \ell(\mathrm{d}z)$$

for bounded measurable functions  $g : \mathbb{R}^{2d} \rightarrow \mathbb{R}$  of bounded support.

*Proof of Lemma S5.* From Daley and Vere-Jones (2003) Chapter 6, we have

$$\begin{aligned}\lambda_X &= \eta_X \lambda_Z, \\ \check{M}_{XZ}(B) &= \check{M}_{\Lambda_X, Z}(B), \\ \check{M}_{XY}(B) &= \check{M}_{\Lambda_X, \Lambda_Y}(B), \\ \check{M}_{XX}(B) &= \check{M}_{\Lambda_X, \Lambda_X}(B) + \lambda_X \delta(B).\end{aligned}$$

The remaining can be obtained by relabelling and symmetry. Proceeding in turn, firstly

$$\begin{aligned}\check{M}_{XZ}(B) &= \check{M}_{\Lambda_X, Z}(B) \\ &= \mathbb{E} \left[ \int_{\mathbb{U}^d} \Lambda_X(B + y) N_Z(dy) \right] \\ &= \eta_X \mathbb{E} \left[ \int_{\mathbb{R}^d} \int_{\mathbb{R}^d} P_X(B + y - x) \mathbb{1}_{\mathbb{U}^d}(y) N_Z(dx) N_Z(dy) \right] \\ &= \eta_X \int_{\mathbb{R}^{2d}} P_X(B + y - x) \mathbb{1}_{\mathbb{U}^d}(y) M_{ZZ}(dx \times dy) \\ &= \eta_X \int_{\mathbb{R}^d} \int_{\mathbb{R}^d} P_X(B - u) \mathbb{1}_{\mathbb{U}^d}(z) \check{M}_{ZZ}(du) \ell(dz) \\ &= \eta_X \int_{\mathbb{R}^d} P_X(B - u) \check{M}_{ZZ}(du).\end{aligned}$$

Secondly

$$\begin{aligned}\check{M}_{XY}(B) &= \check{M}_{\Lambda_X, \Lambda_Y}(B) \\ &= \mathbb{E} \left[ \int_{\mathbb{U}^d} \Lambda_X(B + y) \Lambda_Y(dy) \right] \\ &= \eta_X \eta_Y \mathbb{E} \left[ \int_{\mathbb{R}^d} \int_{\mathbb{R}^d} \int_{\mathbb{R}^d} P_X(B + y - x) \mathbb{1}_{\mathbb{U}^d}(y) N_Z(dx) P_Y(dy - z) N_Z(dz) \right] \\ &= \eta_X \eta_Y \mathbb{E} \left[ \int_{\mathbb{R}^d} \int_{\mathbb{R}^d} \int_{\mathbb{R}^d} P_X(B + y' + z - x) \mathbb{1}_{\mathbb{U}^d}(y' + z) N_Z(dx) P_Y(dy') N_Z(dz) \right] \\ &= \eta_X \eta_Y \int_{\mathbb{R}^{2d}} \int_{\mathbb{R}^d} P_X(B + y' + z - x) \mathbb{1}_{\mathbb{U}^d}(y' + z) P_Y(dy') M_{ZZ}(dx \times dz) \\ &= \eta_X \eta_Y \int_{\mathbb{R}^d} \int_{\mathbb{R}^d} \int_{\mathbb{R}^d} P_X(B + y' - u) \mathbb{1}_{\mathbb{U}^d}(y' + z) P_Y(dy') \check{M}_{ZZ}(du) \ell(dz) \\ &= \eta_X \eta_Y \int_{\mathbb{R}^d} \int_{\mathbb{R}^d} \int_{\mathbb{R}^d} P_X(B + y' - u) \mathbb{1}_{\mathbb{U}^d}(z') \ell(dz') P_Y(dy') \check{M}_{ZZ}(du) \\ &= \eta_X \eta_Y \int_{\mathbb{R}^d} \int_{\mathbb{R}^d} P_X(B + y' - u) P_Y(dy') \check{M}_{ZZ}(du).\end{aligned}$$

Finally by a similar argument

$$\check{M}_{XX}(B) = \eta_X \lambda_Z \delta(B) + \eta_X^2 \int_{\mathbb{R}^d} \int_{\mathbb{R}^d} P_X(B + y' - u) P_X(dy') \check{M}_{ZZ}(du).$$

□

*Proof of Lemma S7.* Note that we have immediately that

$$\begin{aligned}\lambda_X \ell(B) &= \eta_X \lambda_Z \ell(B) \\ &= \eta_X \lambda_Z \int_{\mathbb{R}^d} \mathbb{1}_B(u) \ell(du) \int_{\mathbb{R}^d} P_X(dx) \\ &= \eta_X \lambda_Z \int_{\mathbb{R}^d} \int_{\mathbb{R}^d} \mathbb{1}_B(u + x) P_X(dx) \ell(du) \\ &= \eta_X \lambda_Z \int_{\mathbb{R}^d} P_X(B - u) \ell(du),\end{aligned}$$

and therefore

$$\begin{aligned}
\check{C}_{XZ}(B) &= \check{M}_{XZ}(B) - \lambda_X \lambda_Z \ell(B) \\
&= \eta_X \int_{\mathbb{R}^d} P_X(B-u) \check{M}_{ZZ}(du) - \eta_X \lambda_Z^2 \int_{\mathbb{R}^d} P_X(B-u) \ell(du) \\
&= \eta_X \int_{\mathbb{R}^d} P_X(B-u) \check{C}_{ZZ}(du),
\end{aligned}$$

Similarly we have

$$\begin{aligned}
\check{C}_{XY}(B) &= \eta_X \eta_Y \int_{\mathbb{R}^d} \int_{\mathbb{R}^d} P_X(B+y'-u) P_Y(dy') \check{C}_{ZZ}(du), \\
\check{C}_{XX}(B) &= \eta_X \lambda_Z \delta(B) + \eta_X^2 \int_{\mathbb{R}^d} \int_{\mathbb{R}^d} P_X(B+y'-u) P_X(dy') \check{C}_{ZZ}(du).
\end{aligned}$$

Therefore, firstly

$$\begin{aligned}
f_{XZ}(k) &= \int_{\mathbb{R}^d} e^{-2\pi i x \cdot k} \check{C}_{XZ}(dx) \\
&= \int_{\mathbb{R}^d} e^{-2\pi i x \cdot k} \eta_X \int_{\mathbb{R}^d} P_X(dx-u) \check{C}_{ZZ}(du) \\
&= \eta_X \int_{\mathbb{R}^d} \int_{\mathbb{R}^d} e^{-2\pi i (x'+u) \cdot k} P_X(dx') \check{C}_{ZZ}(du) \\
&= \eta_X \phi_X(-k) f_{ZZ}(k) \\
&= \eta_X \overline{\phi_X(k)} f_{ZZ}(k).
\end{aligned}$$

Secondly,

$$\begin{aligned}
f_{XY}(k) &= \int_{\mathbb{R}^d} e^{-2\pi i x \cdot k} \check{C}_{XY}(dx) \\
&= \int_{\mathbb{R}^d} e^{-2\pi i x \cdot k} \eta_X \eta_Y \int_{\mathbb{R}^d} \int_{\mathbb{R}^d} P_X(dx+y'-u) P_Y(dy') \check{C}_{ZZ}(du) \\
&= \eta_X \eta_Y \int_{\mathbb{R}^d} \int_{\mathbb{R}^d} e^{-2\pi i (x'-y'+u) \cdot k} P_X(dx') P_Y(dy') \check{C}_{ZZ}(du) \\
&= \eta_X \eta_Y \overline{\phi_X(k)} \phi_Y(k) f_{ZZ}(k).
\end{aligned}$$

Finally, again by the same logic

$$f_{XX}(k) = \eta_X \lambda_Z + \eta_X^2 |\phi_X(k)|^2 f_{ZZ}(k)$$

□

*Proof of Proposition S4.* Using Lemma S7, note a couple of useful relationships

$$\begin{aligned}
f_{XX}(k) &= \lambda_X + |f_{XZ}(k)|^2 / f_{ZZ}(k) \\
f_{XY}(k) &= f_{XZ}(k) f_{ZY}(k) / f_{ZZ}(k) \\
|f_{XY}(k)|^2 &= (f_{XX}(k) - \lambda_X) (f_{YY}(k) - \lambda_Y)
\end{aligned}$$

Therefore

$$\begin{aligned}
f_{XY \bullet Z}(k) &= f_{XY}(k) - f_{XZ}(k) f_{ZZ}(k)^{-1} f_{ZY}(k) \\
&= f_{XY}(k) - f_{XY}(k) \\
&= 0.
\end{aligned}$$

Next, consider

$$\begin{aligned}
f_{X,Z \bullet Y}(k) &= f_{XZ}(k) - f_{XY}(k)f_{YY}(k)^{-1}f_{Y,Z}(k) \\
&= \eta_X \overline{\phi_X(k)} f_{ZZ}(k) - \frac{\eta_X \eta_Y \overline{\phi_X(k)} \phi_Y(k) \eta_Y \overline{\phi_Y(k)} f_{ZZ}(k)^2}{\eta_Y \lambda_Z + \eta_Y^2 |\phi_Y(k)|^2 f_{ZZ}(k)} \\
&= \eta_X \overline{\phi_X(k)} f_{ZZ}(k) - \frac{\eta_X \eta_Y \overline{\phi_X(k)} |\phi_Y(k)|^2 f_{ZZ}(k)^2}{\lambda_Z + \eta_Y |\phi_Y(k)|^2 f_{ZZ}(k)} \\
&= \frac{\eta_X \lambda_Z \overline{\phi_X(k)} f_{ZZ}(k)}{\lambda_Z + \eta_Y |\phi_Y(k)|^2 f_{ZZ}(k)}
\end{aligned}$$

Now letting  $W = (Y, Z)^\top$ , we have omitting the “ $(k)$ ” for clarity

$$\begin{aligned}
f_{X,X \bullet W} &= f_{XX} - f_{X,W} f_{W,W}^{-1} f_{W,X} \\
&= f_{XX} - [f_{XY} \ f_{XZ}] \begin{bmatrix} f_{YY} & f_{Y,Z} \\ f_{ZY} & f_{ZZ} \end{bmatrix}^{-1} \begin{bmatrix} f_{Y,X} \\ f_{Z,X} \end{bmatrix} \\
&= f_{XX} - \frac{|f_{XY}|^2 f_{ZZ} + |f_{XZ}|^2 f_{YY} - 2 \operatorname{Re}\{f_{XZ} f_{ZY} f_{Y,X}\}}{f_{YY} f_{ZZ} - |f_{Y,Z}|^2} \\
&= f_{XX} - \frac{|f_{XY}|^2 f_{ZZ} + |f_{XZ}|^2 f_{YY} - 2 |f_{XY}|^2 f_{ZZ}}{\lambda_Y f_{ZZ}}.
\end{aligned}$$

Now

$$\begin{aligned}
|f_{XZ}|^2 f_{YY} &= |f_{XZ}|^2 \lambda_Y + |f_{XZ}|^2 |f_{Y,Z}|^2 / f_{ZZ} \\
&= |f_{XZ}|^2 \lambda_Y + |f_{XY}|^2 f_{ZZ}
\end{aligned}$$

and therefore

$$\begin{aligned}
f_{X,X \bullet W} &= f_{XX} - \frac{|f_{XZ}|^2}{f_{ZZ}} \\
&= \lambda_X.
\end{aligned}$$

Finally, we have letting  $U = (Y, X)^\top$

$$\begin{aligned}
f_{Z,Z \bullet U} &= f_{ZZ} - \frac{|f_{ZY}|^2 f_{XX} + |f_{Z,X}|^2 f_{YY} - 2 \operatorname{Re}\{f_{Z,X} f_{XY} f_{Y,Z}\}}{f_{YY} f_{XX} - |f_{Y,X}|^2} \\
&= f_{ZZ} - \frac{2 f_{XX} f_{YY} f_{ZZ} - \lambda_X f_{YY} f_{ZZ} - \lambda_Y f_{XX} f_{ZZ} - 2 |f_{XY}|^2 f_{ZZ}}{f_{YY} f_{XX} - |f_{Y,X}|^2} \\
&= \frac{\lambda_X f_{YY} f_{ZZ} + \lambda_Y f_{XX} f_{ZZ}}{f_{YY} f_{XX} - |f_{Y,X}|^2} - f_{ZZ} \\
&= f_{ZZ} \frac{\lambda_X f_{YY} + \lambda_Y f_{XX} - f_{YY} f_{XX} + |f_{Y,X}|^2}{f_{YY} f_{XX} - |f_{Y,X}|^2} \\
&= f_{ZZ} \frac{\lambda_X f_{YY} + \lambda_Y f_{XX} - f_{YY} f_{XX} + (f_{XX} - \lambda_X)(f_{YY} - \lambda_Y)}{f_{YY} f_{XX} - |f_{Y,X}|^2} \\
&= f_{ZZ} \frac{\lambda_X \lambda_Y}{f_{YY} f_{XX} - |f_{Y,X}|^2} \\
&= f_{ZZ} \frac{\lambda_X \lambda_Y}{\lambda_X f_{YY} + \lambda_Y f_{XX} - \lambda_X \lambda_Y} \\
&= \frac{f_{ZZ} \lambda_Z^2 \eta_X \eta_Y}{\lambda_Z \eta_X \eta_Y^2 |\phi_Y|^2 f_{ZZ} + \lambda_X \lambda_Y + \lambda_Z \eta_Y \eta_X^2 |\phi_X|^2 f_{ZZ} + \lambda_X \lambda_Y - \lambda_X \lambda_Y} \\
&= \frac{f_{ZZ} \lambda_Z}{\eta_Y |\phi_Y|^2 f_{ZZ} + \eta_X |\phi_X|^2 f_{ZZ} + \lambda_Z}
\end{aligned}$$

□

## S5 Simulation study details

### S5.1 Bivariate examples

The first model was constructed by  $Y$  points being a Poisson process, with a child processes of type  $X_0$  having an average of  $\text{Poisson}(\eta_{X_0})$  with the offset between children and the parent, say  $D_{X_0}$ , following a multivariate Gaussian distribution. In particular,  $\lambda_Y = 0.01$ ,  $\eta_{X_0} = 3$ , and  $D_{X_0} \sim \mathcal{N}(0, 1.5^2 I)$ . We then label  $X = X_0$ .

To generate the second model, we start with the same setup as the previous model (for  $Y$  and  $X_0$ ). We then generate the new  $X$  points by again taking clusters, now centred around points of type  $X_0$ , with  $\eta_X = 1$ , and the additional offset  $D_X \sim \mathcal{N}(0, I)$ . The parameters for  $Y$  and  $X_0$  are kept the same as the first example here.

Finally, for the third scenario, we again start with a similar initial  $Y, X_0$  setup, and then  $X$  is set to be the survivors of a thinning process. In particular, each point of type  $X_0$  is assigned a mark uniformly on  $[0, 1]$ . Then if two points are within a distance  $r_X$  of each other, the point with the smaller mark is removed with probability  $1 - p_X$ . For the specific example, we use  $\eta_{X_0} = 15$ , and  $D_{X_0} \sim \mathcal{N}(0, 1.5^2 I)$ ,  $r_X = 3$  and  $p_X = 0.1$ . The parameters for  $Y$  are the same as for the first example.

### S5.2 Trivariate examples

In the trivariate case, we start with a homogeneous Poisson process  $Z$ . In all three cases, we set  $\lambda_Z = 0.01$ .

For the first setting, we generate points of type  $X$  as described in the previous section, with  $\eta_X = 3$  and  $D_X \sim \mathcal{N}(0, 2^2 I)$ . Points of type  $Y$  are generated in the same way, but independently of points of type  $Z$ .

For the second setting, we generate points of type  $Z$  and  $Y$  as just described. Points of type  $X$  were then generated by placing clusters around points of type  $Y$  with  $\eta_X = 1$  and  $D_X \sim \mathcal{N}(0, 2^2 I)$ .

In the final case, points of type  $Z$  and  $Y$  are again generated as in the first example. We then generate points of type  $X_0$  centred at points of type  $Z$  with  $\eta_{X_0} = 10$  and  $D_{X_0} \sim \mathcal{N}(0, 2^2 I)$ . We then conditionally thin them based on their distance to points of type  $Y$ , with survival probability  $p_X = 0.1$  and inhibition radius  $r_X = 3$ .

## S6 Additional simulation results

### S6.1 Example accounting for covariates

Figure 7 shows an example of a trivariate system where the  $Z$  process is inhomogeneous, with intensity  $\lambda_Z([z_1, z_2]) = 0.02z_1/100$  over the region  $[0, 100]^2$ . We then consider the partial  $L$  functions between each pair of processes, accounting for the other process and the intensity (which we treat as known for both the  $L$  and partial  $L$  functions). For example, when considering  $X$  vs  $Y$ , we account for the point pattern  $Z$  and the covariate  $\lambda_Z$ .<sup>7</sup> Again we plot the three different interaction scenarios. We see that even in this inhomogeneous setting, we are still able to recover the underlying structure using the partial  $L$  function. In particular, the inhomogeneous  $L$  function discovers clustering in almost all cases (except between  $Y$  and  $Z$  in the agnostic offspring case, where there should be clustering). In contrast, the partial  $L$  function correctly recovers the same structure as that seen in the corresponding example in the main manuscript.

### S6.2 Pair correlation functions from examples

Figures 8 and 9 show the pair correlation functions corresponding to the example processes in the main manuscript.

### S6.3 Debiasing comparison

For a simple example, Fig. 10 shows the average of both the simple plug in estimator and the debiased estimator as well as the true  $L$  function, for the first models considered in the trivariate simulation, for the partial  $L$  function of the  $X$  process with itself. We can see that even in this simple case the biased estimate has a substantial artifact at low radii that is not present in the true or debiased version.

<sup>7</sup>Strictly speaking, this violates the assumption that the processes are jointly homogeneous. However, the partial  $L$  function does recover the structure in this case, and the relationships between processes are still the invariant to shifts, even though the intensity is deterministic.

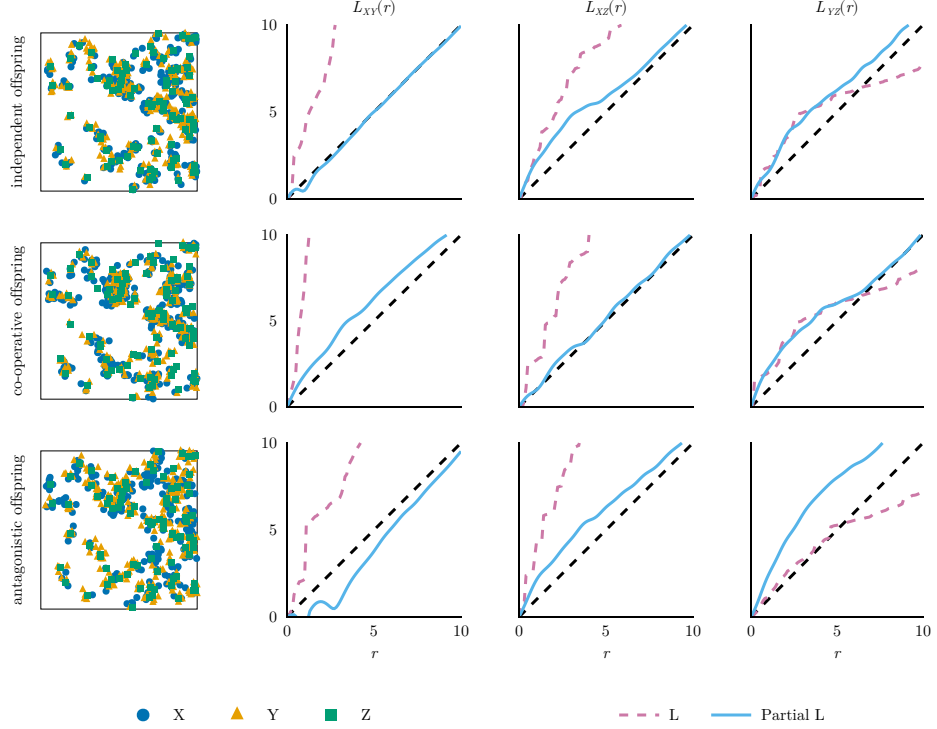


Figure 7: An inhomogeneous version of the trivariate examples. We again show the same trivariate system with three different interaction types, but now the intensity of the base process  $Z$  is not constant. The first column shows example processes, the second column shows the  $L$  function and partial  $L$  function between process  $X$  and process  $Y$  (accounting for  $Z$  and  $\lambda_Z$ ), the third column shows interactions between  $X$  and  $Z$  (accounting for  $Y$  and  $\lambda_Z$ ) and the final column shows interactions between  $Y$  and  $Z$  (accounting for  $X$  and  $\lambda_Z$ ).

#### S6.4 Comparison of L function computation from spectra to direct methods

Another important thing to consider is the accuracy of the  $L$  function computed via the spectral method compared to direct methods. To investigate this, we compare standard border correction estimates of the  $L$  function to those computed via the spectral method for standard univariate point processes. In particular, we consider a Poisson processes, three different Thomas processes with varying cluster sizes, and a Matern hard core II process with varying inhibition radii. The  $L$  functions of each of these models are shown in Fig. 11.

We will compare the standard border corrected estimate of the  $L$  function to those computed with both of the different spectral methods proposed in this work (direct and pre-rotationally averaged). We will also vary the wavenumber grid size used in the spectral methods. In particular, we consider grids of size  $25 \times 25$ ,  $50 \times 50$ ,  $100 \times 100$ , and a recommended grid size based on spacing scaling with the region size, as recommended in the main manuscript. In all cases, we used a highest wavenumber based on the underlying true spectra, ensuring that we cover wavenumbers at which there is meaningful shape in the corresponding model spectra.

We then simulate 100 realisations of each model over increasing square windows of size  $[0, L]^2$  for  $L = 100, 150, 200, 250, 300$ . We then compute average mean squared error and bias of the estimates, averaged accross all the radii considered. We show the relative mean squared error, bias and timings in Fig. 12. The quantities are displayed relative to the border corrected estimate, so that we show  $\log_{10}(\text{MSE}_{\text{method}}/\text{MSE}_{\text{border}})$  and  $\log_{10}(|\text{Bias}_{\text{method}}|/|\text{Bias}_{\text{border}}|)$ .

We see that in almost all cases, the spectral methods outperform the border corrected estimate in terms of mean squared error, with the exception of the Matern with the largest inhibition radius considered. Even then, the spectral methods are competitive, which is our main goal. Furthermore, we see that the rotationally averaged method tends to outperform the direct spectral method, particularly at smaller grid sizes. This further justifies the use and development of this method in the main manuscript, as it is more robust in simulations than our initial approach.

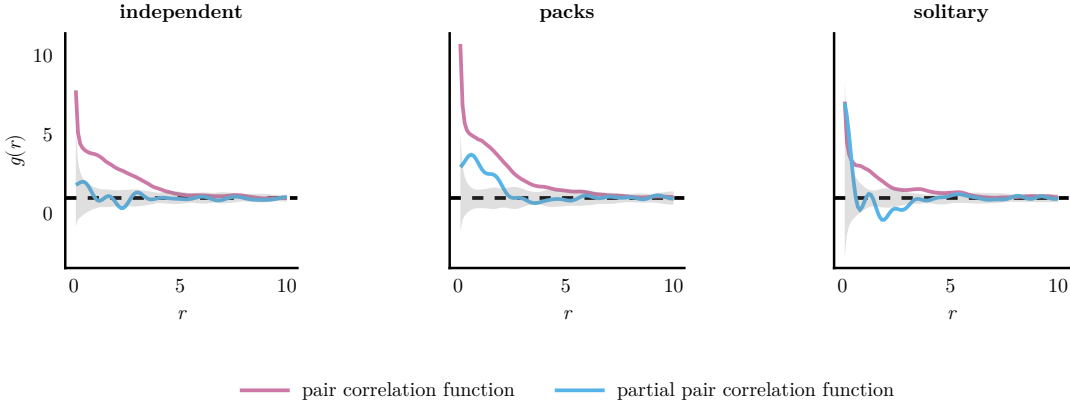


Figure 8: The pair correlation function and partial pair correlation function between the predator process ( $X$ ) in the latter case accounting for the prey process ( $Y$ ). The left column shows the first scenario, where the predators do not interact with each other. The middle column shows the second scenario, where the predators hunt in packs. The right column shows the third scenario, where the predators do not like to be near each other. The envelopes are 95% confidence envelopes using the MAD envelopes proposed by Myllymäki et al. (2017).

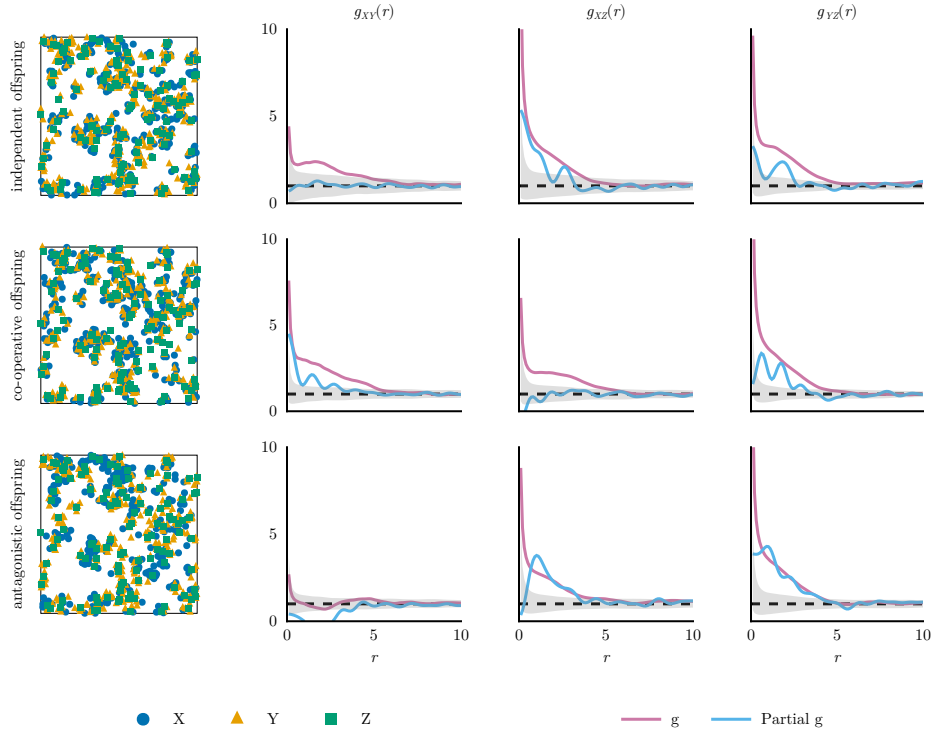


Figure 9: Example of a trivariate system with three different interaction types. The first column shows example processes, the second column shows the pair correlation function and partial pair correlation function between process  $X$  and process  $Y$  (possibly accounting for process  $Z$ ), the third column shows interactions between  $X$  and  $Z$  (accounting for  $Y$ ) and the final column shows interactions between  $Y$  and  $Z$  (accounting for  $Z$ ).

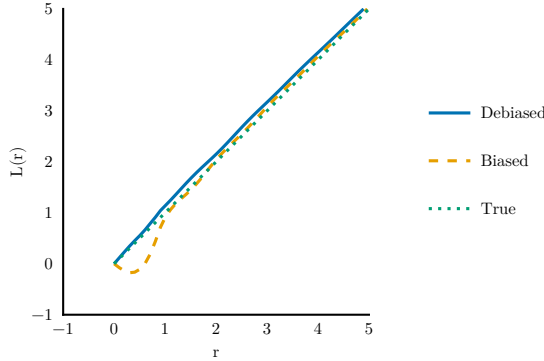


Figure 10: The average estimated  $L_{XX \bullet Y, Z}$  for the first trivariate model considered in the main manuscript. We show the true value, the average of the biased estimate and the average of the debiased estimate (averaged over 100 simulations).

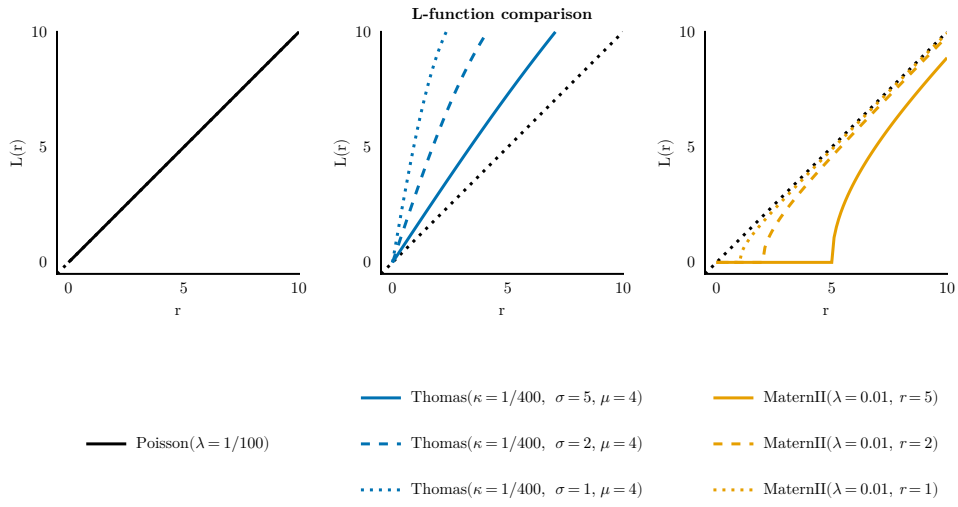


Figure 11: The  $L$  functions for the models used in Section S6.4 to compare the spectral and direct methods.

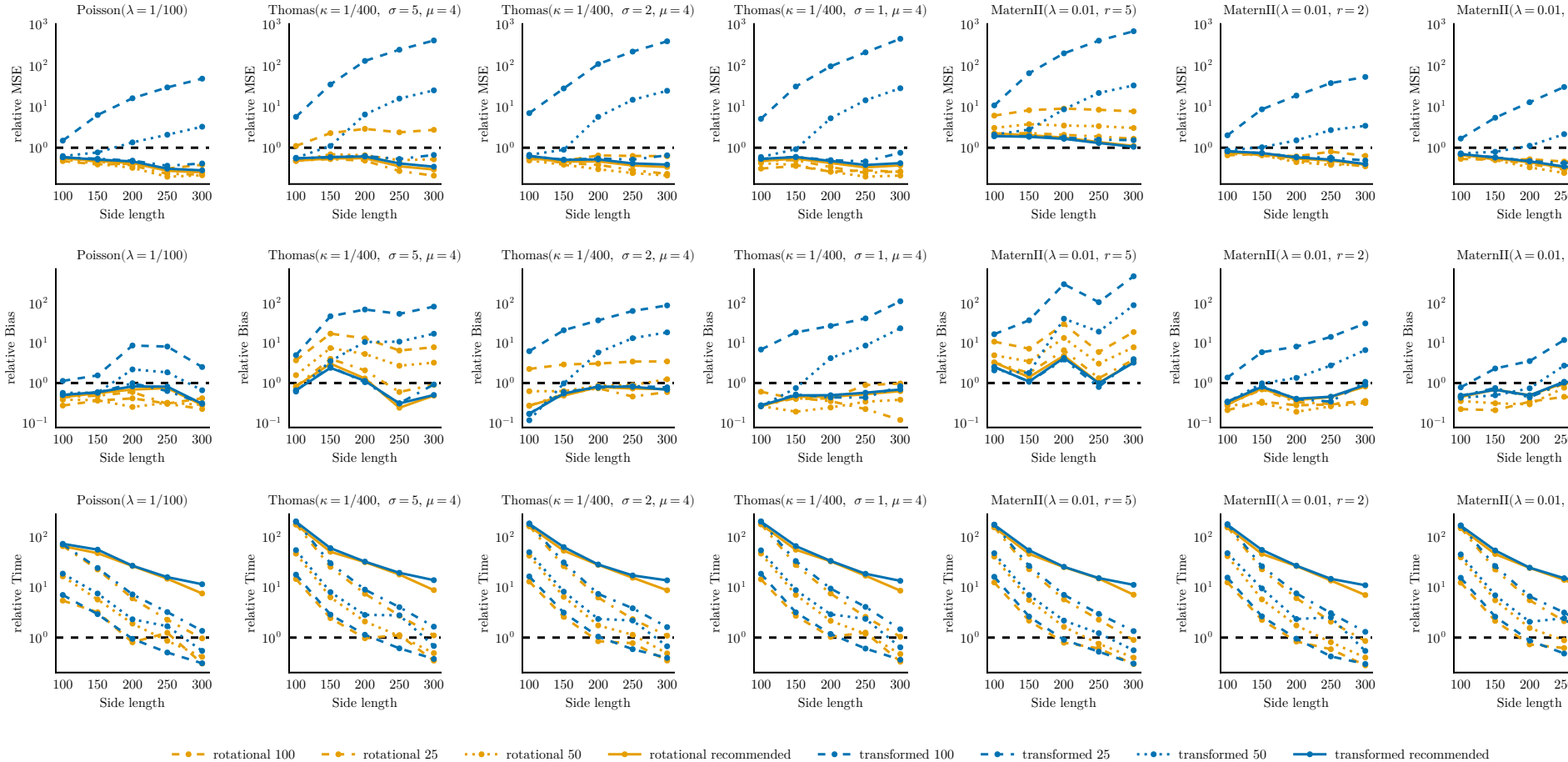


Figure 12: The relative mean squared error, bias and timings of the  $L$  function estimates computed via the spectral methods compared to the border corrected estimate, for different wavenumber grid sizes. The models are the same as those shown in Fig. 11.

## References

Abramowitz, M. and Stegun, I. A. (1948). *Handbook of mathematical functions with formulas, graphs, and mathematical tables*, volume 55. US Government printing office.

Andersen, H., Højbjerre, M., Sørensen, D., and Eriksen, P. (1995). The complex wishart distribution and the complex  $u$ -distribution. In *Linear and Graphical Models: For the Multivariate Complex Normal Distribution*, pages 39–66. Springer.

Baba, K., Shibata, R., and Sibuya, M. (2004). Partial correlation and conditional correlation as measures of conditional independence. *Australian & New Zealand Journal of Statistics*, 46(4):657–664.

Baddeley, A., Møller, J., and Pakes, A. G. (2008). Properties of residuals for spatial point processes. *Annals of the Institute of Statistical Mathematics*, 60(3):627–649.

Baddeley, A., Rubak, E., and Turner, R. (2015). *Spatial Point Patterns: Methodology and Applications with R*. Chapman and Hall/CRC Press, London.

Baddeley, A. and Silverman, B. W. (1984). A cautionary example on the use of second-order methods for analyzing point patterns. *Biometrics*, pages 1089–1093.

Baddeley, A. and Turner, R. (2005). Spatstat: an R package for analyzing spatial point patterns. *Journal of statistical software*, 12:1–42.

Baddeley, A., Turner, R., Møller, J., and Hazelton, M. (2005). Residual analysis for spatial point processes (with discussion). *Journal of the Royal Statistical Society Series B: Statistical Methodology*, 67(5):617–666.

Baddeley, A. J., Møller, J., and Waagepetersen, R. (2000). Non-and semi-parametric estimation of interaction in inhomogeneous point patterns. *Statistica Neerlandica*, 54(3):329–350.

Ben-Israel, A. and Greville, T. N. (2003). *Generalized inverses: theory and applications*. Springer.

Besag, J. (1977). Contribution to the discussion on Dr Ripley's paper. *JR Stat Soc B*, 39:193–195.

Billingsley, P. (2012). *Probability and Measure*. John Wiley & Sons.

Brillinger, D. (1972). The spectral analysis of stationary interval functions. *Proceedings of the 6th Berkeley Symposium on Mathematical Statistics and Probability*, 1.

Brillinger, D. R. (1974). *Time Series: Data Analysis and Theory*. International series in decision processes. Holt, Rinehart, and Winston, New York.

Carlson, D., Haynsworth, E., and Markham, T. (1974). A generalization of the Schur complement by means of the Moore–Penrose inverse. *SIAM Journal on Applied Mathematics*, 26(1):169–175.

Ciarlet, P. G., Miara, B., and Thomas, J.-M. (1989). *Introduction to numerical linear algebra and optimisation*. Cambridge university press.

Dahlhaus, R. (2000). Graphical interaction models for multivariate time series. *Metrika*, 51:157–172.

Daley, D. J. and Vere-Jones, D. (2003). *An Introduction to the Theory of Point Processes, Volume I: Elementary Theory and Methods*. Springer.

Daley, D. J. and Vere-Jones, D. (2007). *An Introduction to the Theory of Point Processes: Volume II: General Theory and Structure*. Springer Science & Business Media.

Dixon, P. M. (2013). *Ripley's K Function*. John Wiley & Sons, Ltd.

Eckardt, M. and Mateu, J. (2019). Analysing multivariate spatial point processes with continuous marks: A graphical modelling approach. *International Statistical Review*, 87(1):44–67.

Eichler, M., Dahlhaus, R., and Sandkühler, J. (2003). Partial correlation analysis for the identification of synaptic connections. *Biological cybernetics*, 89(4):289–302.

Gerrard, D. J. (1969). *Competition quotient: a new measure of the competition affecting individual forest trees*, volume 20. Agricultural Experiment Station, Michigan State University.

Grainger, J. P. (2025a). Jakegrainger/code\_for-the\_partial\_k\_function.

Grainger, J. P. (2025b). Spatialmultitaper.jl.

Grainger, J. P., Rajala, T. A., Murrell, D. J., and Olhede, S. C. (2025). Spectral estimation for spatial point processes and random fields. arXiv preprint arXiv:2312.10176.

Guinness, J., Fuentes, M., Hesterberg, D., and Polizzotto, M. (2014). Multivariate spatial modeling of conditional dependence in microscale soil elemental composition data. *Spatial Statistics*, 9:93–108.

Illian, J., Penttinen, A., Stoyan, H., and Stoyan, D. (2008). *Statistical Analysis and Modelling of Spatial Point Patterns*. John Wiley & Sons.

Medkour, T., Walden, A. T., and Burgess, A. (2009). Graphical modelling for brain connectivity via partial coherence. *Journal of neuroscience methods*, 180(2):374–383.

Møller, J. and Waagepetersen, R. P. (2003). *Statistical Inference and Simulation for Spatial Point Processes*. CRC press.

Mrkvička, T., Dvořák, J., Gonzalez, J. A., and Mateu, J. (2021). Revisiting the random shift approach for testing in spatial statistics. *Spatial Statistics*, 42:100430.

Murrell, D. J. (2010). When does local spatial structure hinder competitive coexistence and reverse competitive hierarchies? *Ecology*, 91(6):1605–1616.

Myllymäki, M., Mrkvička, T., Grabarnik, P., Seijo, H., and Hahn, U. (2017). Global envelope tests for spatial processes. *Journal of the Royal Statistical Society Series B: Statistical Methodology*, 79(2):381–404.

Ripley, B. D. (1977). Modelling spatial patterns. *Journal of the Royal Statistical Society: Series B (Methodological)*, 39(2):172–192.

Teichmann, J., Ballani, F., and van den Boogaart, K. G. (2013). Generalizations of Matérn’s hard-core point processes. *Spatial Statistics*, 3:33–53.

Thomas, M. (1949). A generalization of Poisson’s binomial limit for use in ecology. *Biometrika*, 36(1/2):18–25.

Thomson, D. (1982). Spectrum estimation and harmonic analysis. *Proceedings of the IEEE*, 70(9):1055–1096.

Walden, A. T. (2000). A unified view of multitaper multivariate spectral estimation. *Biometrika*, 87(4):767–788.